Computation of macroscopic permeability of doubly porous media with FFT based numerical homogenization method

Sarra Mezhoud, Vincent Monchiet, Daniel Grande, Michel Bornert

Computation of macroscopic permeability of doubly porous media with FFT based numerical homogenization method

Sarra Mezhoud [a,b] Vincent Monchiet [a] Daniel Grande [b]
Michel Bornert [c]

[a] *Laboratoire Modélisation et Simulation Multi Echelle (MSME), UMR8208 CNRS, Université Paris-Est, 5 boulevard Descartes, 77454 Marne la Vallée Cedex, France*

[b] *Institut de Chimie et des Matériaux Paris-Est (ICMPE), UMR 7182 CNRS, Université Paris-Est, 2 rue Henri Dunant, 94320 Thiais, France*

[c] *Université Paris-Est, Laboratoire Navier, CNRS UMR 8205, ENPC, IFSTTAR, 6/8 avenue Blaise Pascal, 77455 Marne-la-Vallée, France*

Abstract

In this paper we provide a FFT algorithm to compute the effective permeability of doubly porous solids constituted of two populations of pores which are different in size. The paper focuses on the resolution of the fluid flow at the intermediate scale, that of the macropores, that requires the resolution of the coupled Darcy/Stokes problem. The permeability associated with the first population of cavities is assumed to be known. A two-field FFT based iterative scheme is derived to compute the solution of the Darcy/Stokes problem. The principle is to reformulate the problem by considering a unique Brinkman equation with different coefficients for the Darcy and the Stokes regions. As a first application, we determine the macroscopic permeability of a porous solid containing circular macropores. The results are compared to analytic expressions and simplified modeling which use an equivalent Darcy medium in place of the macropores. Next, we apply the FFT method to a bi-porous polymer. The computations are performed on 2D and 3D cells extracted from X-ray computed microtomography.

Key words: Permeability, biporous, Homogenization, Fast Fourier Transform, Darcy, Brinkman

1 Introduction

The design, characterization and simulation in complex hierarchical porous materials has received particular attention for various applications in science and engineering. For instance, hierarchically structured porous media possess large surface area for reaction active sites at different pore scales (see for instance Sun et al. (69), Li et al. (34) and various references herein). Polymer-based porous materials have particularly attracted much interest from the research community (74; 59), as they can easily be functionalized by simple organic reactions. The preparation and analysis of doubly porous materials have particularly attracted the focus of researchers, such as for the design of biocompatible scaffolds meant for biomedical applications (35). Complex multiporous microstructured media can be found in natural materials, biological systems, living organism which are maintained by the mass and energy transfer through the porous system (see (68)). Other applications is the modelling of karstic aquifers that are sometimes represented as multiporosity systems (27; 28). The characterization of flow in such complex microstructure is of key importance for their understanding. The characterization, identification of such microstructures could be also made with the development of homogenization approaches and robust numerical methods to simulate the fluid flow and to determine the mass transfer properties.
The development of homogenization techniques applied to fractured multiporous materials has been the subject of many works during the 90's (see Auriault and Boutin (2; 3; 4), Royer et al. (62), Boutin et al. (13), Olny and Boutin (56)). The approach is based on the asymptotic expansion method first introduced by Sanchez-Palencia (65; 66) and Bensoussan et al. (10). The reader could also refer to the book of Hornung (25) for the application of the homogenization approaches to multiporous solids. When the fractures are large behind the micropores, a double upscaling approach is justified and the macroscopic mass transfer properties are determined by solving the Darcy/Stokes coupled problem at the intermediate scale. The Darcy equation is used to describe the fluid flow in the initially porous structure, and the Stokes equations is related to the fluid flow in the fractures. Numerous studies have concerned the resolution of coupled Darcy/Stokes with various practical applications such as fractured reservoir (57), spontaneous ignition of coal stockpiles (64), modeling of lung alveolar sheet (70), insulation by permeable materials (40), flow through porous bearings or spheres (29; 26), packed bed of particles (37; 52; 53), convection in porous materials (8; 9), modeling of liquid infusion into fibrous media undergoing compaction (58), flow in porous media with cracks (11), industrial filtration systems (24), etc.
Essentially, two strategies have been used considering the Beaver-Joseph-Saffman (BJS) interfacial model (7; 63) or the Brinkman equation (15; 16). From a practical viewpoint, the Brinkman model can simply be regarded as a transmission model, bridging the limits of open to very porous media, described by Stokes

and Darcy's law, respectively. Specifically, by considering the fluid as a porous medium with very high permeability, the fluid/porous composite region can be treated with only the Brinkman equation, which helps circumventing the use of suitable conditions for the interface.

An analytic estimate of the macroscopic permeability has been provided by Markov et al.(39) introducing the concept of equivalent permeability for the macropore. The permeability is determined by solving the coupled Darcy/Stokes equations with the BJS interface model for an isolated cavity embedded in an infinite porous matrix, considering a cylindrical or spherical pore fulfilled by a viscous fluid. The results have been extended to the case of a spheroidal cavity by Rasoulzadeh et al. (61). Another analytic solutions has been derived by Silva and Ginzburg (67) for a composite cylinder, *i.e.* two concentric cylinders in which the flow obeys to the Brinkman equation but with different coefficients in the core and in the coating.

The numerical resolution of the Darcy/Stokes coupled problem has been the subject of intense research. Incompressible fluid flow problems generally contain velocity and pressure as the unknown variables and fall in the category of mixed formulations (77). It was recognized that the solutions strongly depend upon the particular pair of velocity and pressure interpolations employed. The spaces of discretization must satisfy the inf-sup condition or Ladyhenskaya-Babuska-Brezzi (LBB condition). This has been discussed for the Stokes problem by Babuska (6), Brezzi (14) and later for the Darcy-Stokes coupled problem with two different strategies. The decoupled strategies use different discretization spaces in the Stokes and the Darcy region (see for instance Layton et al. (33), Discacciati et al. (20), Celle et al. (18)). Unified finite element approaches are based on the same finite element spaces for both regions by considering robust elements or modified variational formulation (1; 19; 31). Stable finite element formulation of coupled Darcy-Stokes-Brinkman problems has been studied for instance by Xie et al. (75).

In the present paper, we provide a Fourier based numerical method for computing the effective permeability of multiporous materials. The method use Green operators and FFT algorithms and has been first introduced in the context of elasticity (50) and has been later extended to the Stokes fluid flow in a porous rigid medium (43). In each region, we assume that the flow is described by the Brinkman equation. The advantage of using the Brinkman equation is that the velocity and traction are continuous across the interface which is compatible with the use of the Fourier series.

2 Determination of the macroscopic permeability of doubly porous media

2.1 The double homogenization problem

Considering a Representative Volume Element (RVE) of a doubly porous solid, both the first and the second porosity are fulfilled by a newtonian viscous fluid with the dynamic viscosity μ. The material contains two scales : l_1 and l_2 which are characteristic of the first and the second porosity. The second porosity is related to the smaller pores while the first porosity refers to the larger pores. Due to the presence of three scales, that of the first and second porosity and the macroscopic scale, a double homogenization approach could be used to determine the filtration property (see Fig. 1). This double homogenization is only possible if the hypothesis of scale separation is satisfied. Denoting by L the characteristic length of the macroscopic scale, that is typically a dimension of the macrostructure, the scale separation is verified if $l_2 << l_1$ and $l_1 << L$. The double homogenization procedure has been already depicted in a series of papers by Auriault and Boutin (2; 3; 4).

The first homogenization procedure consists in determining the equivalent Darcy solid in replacement of the second porosity. This problem has been well documented in the literature, the reader could see for instance the book of Auriault et al. (5) which contains herein various references about the numerical determination of the permeability. In the present study, we suppose that the permeability of the microporous solid is known (identified experimentally or numerically), and we also assume that it is isotropic for simplicity, the extension to the case of an anisotropic microporous material is not a difficulty. Note that the determination of permeability of monoporous solids with the FFT method has been tackled in (43; 38).

At the intermediate scale, the macropores are embedded in the equivalent Darcy solid. The fluid flow obeys to the Darcy equation in the microporous solid and to the Stokes equation in the macropores. The macroscopic permeability is then determined by solving at the intermediate scale the coupled Darcy/Stokes equations that is detailed in the next section.

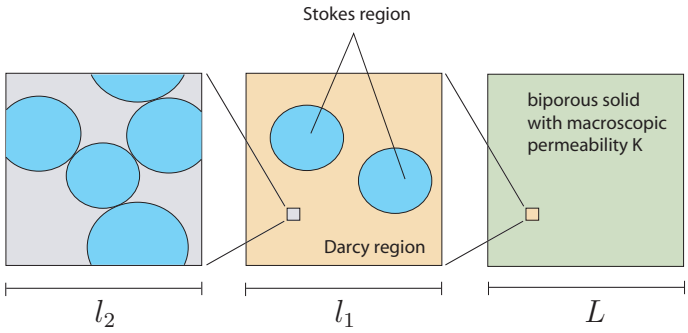

Fig. 1. Three scales of the double homogenization problem of the biporous solid.

2.2 Coupled Darcy/Stokes problem

The determination of the macroscopic permeability of doubly porous media involves the resolution of the coupled Darcy-Stokes equations at the intermediate scale. The macropores or fractures volume is denoted Ω_p and the porous solid volume is denoted Ω_s. The fluid flow is generated by applying the constant pressure gradient $\boldsymbol{J}$. In the macropores, the Stokes equations are used:

$$\begin{aligned} &\mu\Delta\boldsymbol{v} - \nabla p = \boldsymbol{J} \quad && \forall \boldsymbol{x} \in \Omega_p \\ &\operatorname{div} \boldsymbol{v} = 0 && \forall \boldsymbol{x} \in \Omega_p \end{aligned} \tag{1}$$

Within the porous solid, the fluid flow obeys to the Darcy law with the incompressibility condition:

$$\begin{aligned} &\boldsymbol{v} = -\frac{k}{\mu}(\nabla p + \boldsymbol{J}) \quad && \forall \boldsymbol{x} \in \Omega_s \\ &\operatorname{div} \boldsymbol{v} = 0 && \forall \boldsymbol{x} \in \Omega_s \end{aligned} \tag{2}$$

In Eqs. (1) to (2), $\boldsymbol{v}$ denote the local velocity, p, the local pressure, μ is the dynamic viscosity and k is the permeability of the microporous solid. We assume that the porous solid containing the micropores is isotropic, then the relation giving the seepage velocity $\boldsymbol{v}$ as function of the pressure gradient only involves the scalar k. It must be noted, that the use of a tensor in the FFT algorithm described in the next of the paper is possible. The hypothesis of isotropy is considered for simplicity.
Between the two regions, the porous solid and the fluid, appropriate interregional conditions must be considered. For example, the Beavers-Joseph-Saffman model (7; 63) is often considered. Another approach consists in using the Brinkman equation with an effective viscosity in the Darcy medium. The

question about the choice of the conditions is more discussed in the next section.
At the boundary of the unit cell the periodicity is considered for the pressure p and the velocity $\boldsymbol{v}$.
The macroscopic velocity is computed by taking the average of the local velocity (see for instance (60)):

$$\boldsymbol{V} =< \boldsymbol{v} >_{\Omega} = \frac{1}{|\Omega|}\int_{\Omega} \boldsymbol{v} dV \tag{3}$$

Due to the linearity of the equations, the macroscopic permeability linearly depends on the applied macroscopic pressure gradient $\boldsymbol{J}$:

$$\boldsymbol{V} = -\frac{1}{\mu}\boldsymbol{K}.\boldsymbol{J} \tag{4}$$

where $\boldsymbol{K}$ is the macroscopic permeability which depends on the two populations of cavities.

2.3 Resolution with the Brinkman equation

The local problem at the intermediate scale uses two different equations: the Stokes ones in the macropores and the Darcy ones in the microporous solid. This constitutes a difficulty for the application of the FFT method because it has been developed for the resolution of heterogeneous problems, i.e. the problems which use the same equations for each phase but with different local properties. For instance, in the problem of elastic composites, the elastic coefficients differ from one phase to another but the elasticity equations are used anywhere in the unit cell. By introducing the concept of polarization, it is possible to use the Green operator in order to put the problem in an integral form given by the Lippmann-Schwinger and to solve it by an iterative scheme. By adopting the Brinkman equation, the coupled Darcy/Stokes equation can be written as an heterogeneous problem:

$$\varphi(\boldsymbol{x})\Delta\boldsymbol{v} - \beta(\boldsymbol{x})\boldsymbol{v} - \nabla p = \boldsymbol{J} \quad \forall \boldsymbol{x} \in \Omega \tag{5}$$

$$\operatorname{div} \boldsymbol{v} = 0 \quad \forall \boldsymbol{x} \in \Omega \tag{6}$$

where $\varphi(\boldsymbol{x})$ and $\beta(\boldsymbol{x})$ are defined by:

$$\varphi(\boldsymbol{x}) = \begin{cases} \mu & \boldsymbol{x} \in \Omega_p \\ \mu_e & \boldsymbol{x} \in \Omega_s \end{cases}, \quad \beta(\boldsymbol{x}) = \begin{cases} 0 & \boldsymbol{x} \in \Omega_p \\ \mu k^{-1} & \boldsymbol{x} \in \Omega_s \end{cases} \tag{7}$$

in which μ_e is the effective dynamic viscosity. The case of a coupled Darcy/Stokes problem corresponds to $\mu_e = 0$. In the exemples provided in this paper, we put $\mu_e = 0$, excepted for the validation with numerical solutions coming from the literature and given in section 5.
A the boundary of the unit cell we assume the periodicity of the velocity $\boldsymbol{v}$ and the antiperiodicity of the traction $\boldsymbol{\sigma}.\boldsymbol{n}$.
The conditions at the interface between the two phases (denoted by S) is the continuity of the velocity field and the traction (see (75)):

$$\boldsymbol{v}^{(s)} = \boldsymbol{v}^{(p)}, \quad \boldsymbol{\sigma}^{(s)}.\boldsymbol{\nu} = \boldsymbol{\sigma}^{(p)}.\boldsymbol{\nu} \quad \forall \boldsymbol{x} \in S \tag{8}$$

where $\boldsymbol{\nu}$ is the normal unit vector taken on S, exponent (s) makes reference to the microporous solid (Ω_s) and exponent (p) to the fluid phase (Ω_p). In Eq. (8), $\boldsymbol{\sigma}$ is the local stress tensor given by:

$$\boldsymbol{\sigma} = 2\varphi(\boldsymbol{x})\boldsymbol{d} - p\boldsymbol{I} \tag{9}$$

and where $\boldsymbol{d}$ is the strain rate tensor defined by:

$$\boldsymbol{d} = \nabla_s \boldsymbol{v} = \frac{1}{2}(\nabla \boldsymbol{v} + \nabla^T \boldsymbol{v}) \tag{10}$$

that is traceless due to incompressibility.
The interface conditions between the two regions play a key role in the determination of the mass transfer properties of the biporous solid. In the present paper, we just consider the simplest conditions involving both the continuity of the velocity and traction. Besides, such conditions are considered in many works, for instance by Silva and Ginzburg (67) and by Xie et al. (75). The consideration of more accurate description of the fluid transfer between the two regions generally involves jump conditions for the velocity and/or the traction. For instance, the Beaver-Joseph-Saffman model (7; 63) involves the jump of the tangential component of the velocity while the normal component remains continuous across the surface between the Darcy and the Stokes region. Alternatively, other works add more terms in the momentum transport equation (54; 55) (see also (23; 71; 72) for the determination of the stress jump coefficient). In these work, the jump condition is constructed to join Darcy region with the Brinkman one and it involves a jump in the stress. Later, in (73), both the jump of the velocity and stress was considered between a porous medium and a fluid. Note also that the interface condition has been recently treated in (36) with a penalization method.
The standard FFT method is better suited to problems with continuous fields since it uses a discretization with Fourier series, both the continuity of the velocity and traction is then considered in this paper. In order to obtain more accurate description, jump conditions will be considered between the porous

solid and the fluid and could be accounted with the extended FFT method recently proposed by Monchiet (48).

2.4 Non dimensional problem

The calculations are performed for the non dimensional problem. The latter is derived by considering the adapted variable change. Without macropores, the solution in the unit cell is trivial, the velocity is constant in the unit cell and given by:

$$\boldsymbol{v} = -\frac{k}{\mu}\boldsymbol{J} \tag{11}$$

If the macropores are interconnected, we non-dimensionalize the velocity with l_1. In that case, the macroscopic velocity is of the order of the square of the characteristic size of the macropore that is approximatively equal to the square of l_1 (if the size of the unit cell and the characteristic size of the macropores are of the same order). In the paper, we only study the case of non-interconnected macropores. This means that the macroscopic permeability is of the order of k, the permeability of the porous matrix (with the micropores), that is also of the same order that the square of l_2. This suggests that the velocity at the intermediate scale is:

$$\boldsymbol{v} = O\left(\frac{k}{\mu}\boldsymbol{J}\right) \tag{12}$$

We then use the change of variables:

$$\boldsymbol{v} = \frac{k|\boldsymbol{J}|}{\mu}\overline{\boldsymbol{v}}, \quad p = |\boldsymbol{J}|l_1\overline{p}, \quad \boldsymbol{J} = |\boldsymbol{J}|\boldsymbol{j}, \quad \boldsymbol{x} = l_1\overline{\boldsymbol{x}} \tag{13}$$

where it is recalled that l_1 is the dimension of the unit cell at the intermediate scale. Vector $\boldsymbol{j}$ gives the direction of the prescribed macroscopic pressure gradient, $\boldsymbol{j} = \boldsymbol{J}/\|\boldsymbol{J}\|$. Introducing this change of variables in Eqs. (5) and (6) leads to:

$$\overline{\varphi}(\overline{\boldsymbol{x}})\overline{\Delta}\overline{\boldsymbol{v}} - \overline{\beta}(\overline{\boldsymbol{x}})\overline{\boldsymbol{v}} - \overline{\nabla}\overline{p} = \boldsymbol{j} \quad \forall\overline{\boldsymbol{x}} \in \overline{\Omega} \tag{14}$$

$$\overline{\mathrm{div}}\overline{\boldsymbol{v}} = 0 \quad \forall\overline{\boldsymbol{x}} \in \overline{\Omega} \tag{15}$$

where $\overline{\varphi}(\overline{\boldsymbol{x}})$ and $\overline{\beta}(\overline{\boldsymbol{x}})$ are defined by:

$$\overline{\varphi}(\overline{\boldsymbol{x}}) = \begin{cases} \varepsilon^2 & \overline{\boldsymbol{x}} \in \overline{\Omega}_f \\ \dfrac{\mu_e}{\mu}\varepsilon^2 & \overline{\boldsymbol{x}} \in \overline{\Omega}_s \end{cases}, \quad \overline{\boldsymbol{\beta}}(\overline{\boldsymbol{x}}) = \begin{cases} 0 & \overline{\boldsymbol{x}} \in \overline{\Omega}_f \\ 1 & \overline{\boldsymbol{x}} \in \overline{\Omega}_s \end{cases} \tag{16}$$

in which we have introduced the non dimensional coefficient ε defined by:

$$\varepsilon = \frac{\sqrt{k}}{l_1} \tag{17}$$

The permeability k is associated with the second porosity and is $k = O(l_2^2)$ where it is recalled that l_2 is the characteristic dimension of the second porosity. Assuming the scale separation between the first and the second porosity, the coefficient ε must remain small behind 1. When ε tends to zero, that corresponds to a strong scale separation between the two populations of pores, the dissipative term in Eq. (14) can be omitted and the problem reduces to solve only the Darcy equation. In that case, the macropores are replaced by an equivalent Darcy medium with a null hydraulic resistivity (an infinite permeability).
Introducing the change of variable (13) in equation (4) with the definition (3) for the macroscopic velocity, we obtain:

$$\overline{\boldsymbol{V}} = -\overline{\boldsymbol{K}}.\boldsymbol{j} \tag{18}$$

in which $\overline{\boldsymbol{K}}$ is given by:

$$\overline{\boldsymbol{K}} = \frac{1}{k}\boldsymbol{K} \tag{19}$$

$\overline{\boldsymbol{K}}$ is a dimensionless permeability. It can be also interpreted as an "amplification factor" due to the presence of the macropores in the microporous matrix. Indeed, if the microporous matrix has the permeability k, the macroscopic permeability is $\boldsymbol{K} = k\overline{\boldsymbol{K}}$. The macroscopic resistivity (the inverse of $\boldsymbol{K}$) is $\boldsymbol{H} = h\overline{\boldsymbol{H}}$ where $h = k^{-1}$ and $\overline{\boldsymbol{H}} = \overline{\boldsymbol{K}}^{-1}$.

3 Mathematic preliminaries

New FFT algorithms are derived in this paper to solve the Brinkman equation. The cornerstone of the FFT method is the formulation of the local problem into an integral equation called Lippmann-Schwinger equation which uses Green operators. This integral equation is established by taking advantage of the solution of an auxiliary problem: the inclusion problem in the sense of Eshelby (21). In this section, we derive the close form solution of the inclusion problem related to the Brinkman problem and we introduce the corresponding Green operators.

3.1 Reformulation of the Brinkman problem

Let us first introduce the vector $\boldsymbol{\omega}$ defined by:

$$\boldsymbol{\omega} = \beta(\boldsymbol{x})\boldsymbol{v} \tag{20}$$

The Brinkman problem is rewritten into the following form:

$$\begin{aligned} \mathrm{div}(\boldsymbol{\sigma}) &= \boldsymbol{\omega} - \boldsymbol{W} && (21)\\ \boldsymbol{\sigma} &= 2\varphi(\boldsymbol{x})\boldsymbol{d} - p\boldsymbol{I} && (22)\\ \boldsymbol{\omega} &= \beta(\boldsymbol{x})\boldsymbol{v} && (23)\\ \boldsymbol{d} &= \nabla_s \boldsymbol{v} && (24)\\ \mathrm{div}(\boldsymbol{v}) &= 0 && (25) \end{aligned}$$

with $\boldsymbol{W} = -\boldsymbol{J}$ and the periodicity condition at the boundary of the unit cell. We observe that the set of equations is constituted of:

- Eq. (21): an equilibrium equation for the stress field $\boldsymbol{\sigma}$ and $\boldsymbol{\omega}$,
- Eqs. (22) and Eq. (23): an uncoupled local linear relation between the pair of tensors $(\boldsymbol{\sigma}, \boldsymbol{\omega})$ and the pair $(\boldsymbol{d}, \boldsymbol{v})$,
- Eq. (24): a compatibility relation between the strain rate tensor and the velocity,
- Eq. (25): the incompressibility condition.

By taking the average of the first equation in (21) over the volume of the unit cell Ω, we obtain:

$$< \mathrm{div}(\boldsymbol{\sigma}) >_\Omega = < \boldsymbol{\omega} >_\Omega - \boldsymbol{W} \tag{26}$$

By making use of the divergence theorem, the first term in the above equation can be transformed into an integral over the boundary of the cell that is null due to the antiperiodicity of the traction. We deduce that:

$$< \boldsymbol{\omega} >_\Omega = \boldsymbol{W} \tag{27}$$

Then, $\boldsymbol{W}$ represents the average of the quantity $\boldsymbol{\omega}$ over the volume Ω. The average of the local velocity reads:

$$\boldsymbol{V} = < \boldsymbol{v} >_\Omega = \frac{1}{\mu}\boldsymbol{K}.\boldsymbol{W} \tag{28}$$

where $\boldsymbol{K}$ is the macroscopic permeability, or equivalently:

$$\boldsymbol{W} = \mu \boldsymbol{H}.\boldsymbol{V} \tag{29}$$

where $\boldsymbol{H}$ is the macroscopic resistivity (the inverse of $\boldsymbol{K}$).
Let us introduce the deviatoric part of the stress tensor denoted by $\boldsymbol{s}$:

$$\boldsymbol{s} = \boldsymbol{\sigma} + p\boldsymbol{I} = 2\varphi(\boldsymbol{x})\boldsymbol{d} \tag{30}$$

The relation between the pair of tensors $(\boldsymbol{s}, \boldsymbol{\omega})$ and $(\boldsymbol{d}, \boldsymbol{v})$ can be put into the form:

$$\left(\begin{array}{c} \boldsymbol{s} \\ \boldsymbol{\omega} \end{array}\right) = \left(\begin{array}{c|c} 2\varphi(\boldsymbol{x}) & 0 \\ \hline 0 & \beta(\boldsymbol{x}) \end{array}\right) \left(\begin{array}{c} \boldsymbol{d} \\ \boldsymbol{v} \end{array}\right) \tag{31}$$

3.2 Inclusion problem

3.2.1 Solution in Fourier space

Let us introduce the fictitious homogeneous Brinkman medium with the coefficients φ_0 and β_0 (the permeability is assumed to be isotropic). We are interested in the following inclusion problem in the sense of Eshelby (21) (see also the book of Mura (51)): the homogeneous porous solid is subjected to the following pair of periodic eigenfields $\boldsymbol{q}$ (with $\mathrm{tr}(\boldsymbol{q}) = 0$) and $\boldsymbol{f}$:

$$\left\{\begin{array}{l} \mathrm{div}(\boldsymbol{\sigma}) = \boldsymbol{\omega} - \boldsymbol{W} \\ \boldsymbol{\sigma} = 2\varphi_0 \boldsymbol{d} - p\boldsymbol{I} + \boldsymbol{q} \\ \boldsymbol{\omega} = \beta_0 \boldsymbol{v} + \boldsymbol{f} \\ \boldsymbol{d} = \nabla_s \boldsymbol{v} \\ \mathrm{div}(\boldsymbol{v}) = 0 \end{array}\right. \tag{32}$$

The solution of this problem could be easily computed in the Fourier space. All the details could be found in appendix A. By adopting the notations introduced in Eq. (31), the solution of the inclusion problem can be read:

$$\left(\begin{array}{c} \widehat{\boldsymbol{d}} \\ \widehat{\boldsymbol{v}} \end{array}\right) = -\left(\begin{array}{c|c} \widehat{\boldsymbol{\Gamma}}^0 & \widehat{\boldsymbol{\Omega}}^0 \\ \hline -\overline{\widehat{\boldsymbol{\Omega}}^0} & \widehat{\boldsymbol{G}}^0 \end{array}\right) \left(\begin{array}{c} \widehat{\boldsymbol{q}} \\ \widehat{\boldsymbol{f}} \end{array}\right) \tag{33}$$

where the "hat" over each variable represent the Fourier transform of the corresponding quantity.
In Eq. (33), we have introduced the following Green operators:

$$\widehat{\Gamma}^0_{ijkl} = \frac{\lambda\|\boldsymbol{\xi}\|^2}{4}(Q_{ip}P_{jq} + Q_{iq}P_{jp} + P_{ip}Q_{jq} + P_{iq}Q_{jp}), \tag{34}$$

$$\widehat{\Omega}^0_{ijk} = \frac{i\lambda\|\boldsymbol{\xi}\|}{2}(Q_{ik}n_j + Q_{jk}n_i), \tag{35}$$

$$\widehat{G}^0_{ij} = \lambda Q_{ij} \tag{36}$$

where λ is defined by:

$$\lambda = \frac{1}{\varphi_0\|\boldsymbol{\xi}\|^2 + \beta_0} \tag{37}$$

and $\boldsymbol{P}$, $\boldsymbol{Q}$, and $\boldsymbol{n}$ are defined by:

$$\begin{array}{l} \forall \boldsymbol{\xi} \neq 0 : \quad \boldsymbol{Q} = \boldsymbol{I} - \boldsymbol{P}, \quad \boldsymbol{P} = \boldsymbol{n} \otimes \boldsymbol{n}, \quad \boldsymbol{n} = \dfrac{\boldsymbol{\xi}}{\|\boldsymbol{\xi}\|}, \\ \text{for } \boldsymbol{\xi} = 0 : \ \boldsymbol{P} = 0, \ \boldsymbol{Q} = 0, \ \boldsymbol{n} = 0 \end{array} \tag{38}$$

Note that tensors $\boldsymbol{P}$ and $\boldsymbol{Q}$ are two projectors. They satisfy to ($\forall \boldsymbol{\xi} \neq 0$):

$$\boldsymbol{P}.\boldsymbol{Q} = \boldsymbol{Q}.\boldsymbol{P} = 0, \quad \boldsymbol{P}.\boldsymbol{P} = \boldsymbol{P}, \quad \boldsymbol{Q}.\boldsymbol{Q} = \boldsymbol{Q}, \quad \boldsymbol{P} + \boldsymbol{Q} = \boldsymbol{I}, \tag{39}$$

$$\boldsymbol{P}.\boldsymbol{n} = \boldsymbol{n}.\boldsymbol{P} = \boldsymbol{n}, \quad \boldsymbol{n}.\boldsymbol{Q} = \boldsymbol{Q}.\boldsymbol{n} = 0 \tag{40}$$

For $\boldsymbol{\xi} = 0$, $\widehat{\boldsymbol{\Gamma}}^0$, $\widehat{\boldsymbol{\Omega}}^0$ and $\widehat{\boldsymbol{G}}^0$ are null. In Eq. (33), $\overline{\widehat{\boldsymbol{\Omega}}^0}$ is the adjoint of $\widehat{\boldsymbol{\Omega}}^0$ such that $\boldsymbol{d} : \widehat{\boldsymbol{\Omega}}^0.\boldsymbol{v} = \boldsymbol{v}.\overline{\widehat{\boldsymbol{\Omega}}^0} : \boldsymbol{d}$.

3.2.2 Solution in real space

Let us come back to the real space. The solution of the inclusion problem is derived by taking the inverse Fourier transform of Eq. (33). Let us recall that the component of any quantity with $\boldsymbol{\xi} = 0$ represents the volume average of this quantity over the volume of the unit cell Ω. As a consequence, when a Green operator is applied to any pair of tensors, it generates a pair of tensors whose volume average is null. Therefore, the average of each corresponding quantity must be added when coming back to the real space:

$$\begin{pmatrix} \boldsymbol{d} \\ \boldsymbol{v} \end{pmatrix} = \begin{pmatrix} \boldsymbol{0} \\ \boldsymbol{V} \end{pmatrix} - \left(\begin{array}{c|c} \boldsymbol{\Gamma}^0 & \boldsymbol{\Omega}^0 \\ \hline -\overline{\boldsymbol{\Omega}^0} & \boldsymbol{G}^0 \end{array}\right) * \begin{pmatrix} \boldsymbol{q} \\ \boldsymbol{f} \end{pmatrix} \tag{41}$$

where "$*$" denotes the convolution product. The mean value of each corresponding quantity has been added: $\boldsymbol{V}$ for the velocity field and zero for the

strain rate tensor $\boldsymbol{d}$ (since the latter derivates from a periodic velocity field). To simplify the notations, we put:

$$\mathcal{G}_0 = \left(\begin{array}{c|c} \boldsymbol{\Gamma}^0 & \boldsymbol{\Omega}^0 \\ \hline -\overline{\boldsymbol{\Omega}^0} & \boldsymbol{G}^0 \end{array}\right) \tag{42}$$

such that the solution of the inclusion problem can be also read:

$$\begin{pmatrix} \boldsymbol{d} \\ \boldsymbol{v} \end{pmatrix} = \begin{pmatrix} \boldsymbol{0} \\ \boldsymbol{V} \end{pmatrix} - \mathcal{G}_0 * \begin{pmatrix} \boldsymbol{q} \\ \boldsymbol{f} \end{pmatrix} \tag{43}$$

4 Resolution with a FFT based iterative scheme

4.1 Lippmann-Schwinger equation

The Brinkman problem (5), (6) can be put into the form (32) by considering the following expression for the pair of eigentensors:

$$\boldsymbol{q} = 2(\varphi(\boldsymbol{x}) - \varphi_0)\boldsymbol{d}, \quad \boldsymbol{f} = (\beta(\boldsymbol{x}) - \beta_0)\boldsymbol{v} \tag{44}$$

By considering expressions (44) in relation (43), we deduce that:

$$\begin{pmatrix} \boldsymbol{d} \\ \boldsymbol{v} \end{pmatrix} = \begin{pmatrix} \boldsymbol{0} \\ \boldsymbol{V} \end{pmatrix} - \mathcal{G}_0 * \begin{pmatrix} 2(\varphi(\boldsymbol{x}) - \varphi_0)\boldsymbol{d} \\ (\beta(\boldsymbol{x}) - \beta_0).\boldsymbol{v} \end{pmatrix} \tag{45}$$

The latter equation is an integral equation, called Lippmann-Schwinger equation, for the variables $\boldsymbol{v}$ and $\boldsymbol{d}$. The enforcing term is the macroscopic velocity $\boldsymbol{V}$.

4.2 Resolution with an iterative scheme: first form

The solution of the integral equation (45) can be expanded along Neumman series along the line of a method first introduced by Brown (17), Kroner (32) and numerically computed with the FFT in the context of elasticity by Moulinec and Suquet (50). Each term of the Neumann series can be computed with the following iterative scheme:

$$\begin{pmatrix} \boldsymbol{d}_{i+1} \\ \boldsymbol{v}_{i+1} \end{pmatrix} = \begin{pmatrix} \boldsymbol{0} \\ \boldsymbol{V} \end{pmatrix} - \mathcal{G}_0 * \begin{pmatrix} 2(\varphi(\boldsymbol{x}) - \varphi_0)\boldsymbol{d}_i \\ (\boldsymbol{\beta}(\boldsymbol{x}) - \beta_0)\boldsymbol{v}_i \end{pmatrix} \tag{46}$$

and which is initialized with:

$$\boldsymbol{d}_0 = 0, \quad \boldsymbol{v}_0 = \boldsymbol{V} \tag{47}$$

Eq. (46) is the first form of the iterative scheme. A second form is provided in the next section.

4.3 Second form of the iterative scheme

A simplification of the iterative scheme (46) is possible. To this purpose, let us consider the following property of the Green operator $\mathcal{G}_0$: for any periodic velocity field $\boldsymbol{v}$ which complies with the incompressibility, we have

$$\mathcal{G}_0 * \begin{pmatrix} 2\varphi_0\boldsymbol{d} \\ \beta_0\boldsymbol{v} \end{pmatrix} = \begin{pmatrix} \boldsymbol{d} \\ \boldsymbol{v} - \boldsymbol{V} \end{pmatrix} \tag{48}$$

in which the strain rate field $\boldsymbol{d}$ derivates from $\boldsymbol{v}$. The demonstration is provided in the appendix (see section B).
Since at each step of the iteration process we have $\boldsymbol{d}_i = \nabla_s \boldsymbol{v}_i$ and $\boldsymbol{v}_i$ is incompressible, it is possible to simplify the iterative scheme (46) by:

$$\begin{pmatrix} \boldsymbol{d}_{i+1} \\ \boldsymbol{v}_{i+1} \end{pmatrix} = \begin{pmatrix} \boldsymbol{d}_i \\ \boldsymbol{v}_i \end{pmatrix} - \mathcal{G}_0 * \begin{pmatrix} 2\varphi(\boldsymbol{x})\boldsymbol{d}_i \\ \beta(\boldsymbol{x})\boldsymbol{v}_i \end{pmatrix} \tag{49}$$

that is the second form of the iterative scheme. The recurrence process is still initialized by Eq. (47). Note that in Eq. (49), $2\varphi(\boldsymbol{x})\boldsymbol{d}_i$ is the deviatoric part of the stress field computed at iteration i and which can be denoted $\boldsymbol{s}_i$. Also, $\beta(\boldsymbol{x})\boldsymbol{v}_i$ can be denoted $\boldsymbol{\omega}_i$. When the convergence of the iterative scheme is achieved, $\boldsymbol{\omega}_i = \beta(\boldsymbol{x})\boldsymbol{v}_i$ is equal to $\boldsymbol{\omega}$ the solution of the Brinkman equation (21)-(25). By taking the average of $\boldsymbol{\omega}$ over the volume of the unit cell, we determine the macroscopic resistivity (and then the macroscopic permeability) following Eq. (29).

4.4 Third form of the iterative scheme

The solution at convergence may comply with all the equations in (21)-(25). Some equations are verified at each step of the iteration process, they are: the local relations $\boldsymbol{s}_i = 2\varphi(\boldsymbol{x})\boldsymbol{d}_i$ and $\boldsymbol{\omega}_i = \beta(\boldsymbol{x})\boldsymbol{v}_i$, the compatibility equation between the strain rate tensor and the velocity field, $\boldsymbol{d}_i = \nabla_s \boldsymbol{v}_i$ and the incompressibility, $\mathrm{tr}(\boldsymbol{d}_i) = \mathrm{div}(\boldsymbol{v}_i) = 0$.
Only the equilibrium $\mathrm{div}(\boldsymbol{\sigma}_i) = \boldsymbol{\omega}_i - \boldsymbol{W}$ is not verified at each iteration but only at the convergence.
When the convergence is achieved, that corresponds to $\boldsymbol{d}_{i+1} = \boldsymbol{d}_i$ and $\boldsymbol{v}_{i+1} = \boldsymbol{v}_i$, we have:

$$\mathcal{G}_0 \begin{pmatrix} \boldsymbol{s}_i \\ \boldsymbol{\omega}_i \end{pmatrix} = 0 \tag{50}$$

The latter condition is a measurement of the distance from the equilibrium. Let us give the proof. To this purpose, let us come back to the Fourier space. Owing to Eq. (42) (with the definitions (34)-(36)), it is easy to show that:

$$\widehat{\mathcal{G}_0} \begin{pmatrix} \widehat{\boldsymbol{s}}_i \\ \widehat{\boldsymbol{\omega}}_i \end{pmatrix} = -\lambda \begin{pmatrix} i\widehat{\boldsymbol{E}_i} \otimes_s \boldsymbol{\xi} \\ \widehat{\boldsymbol{E}_i} \end{pmatrix} \tag{51}$$

where $\widehat{\boldsymbol{E}_i}$ is given by:

$$\widehat{\boldsymbol{E}_i} = \boldsymbol{Q}.(i\widehat{\boldsymbol{s}}_i.\boldsymbol{\xi} - \widehat{\boldsymbol{\omega}}_i) \tag{52}$$

It can be noted that the quantity $\widehat{\boldsymbol{E}_i}$ is null when the equilibrium is verified. Indeed, the equilibrium is $i\widehat{\boldsymbol{\sigma}}_i.\boldsymbol{\xi} = \widehat{\boldsymbol{\omega}}_i$ in the Fourier space. The projection of this equation onto the plane normal to the wave vector $\boldsymbol{\xi}$ is $i\boldsymbol{Q}.\widehat{\boldsymbol{s}}_i.\boldsymbol{\xi} = \boldsymbol{Q}.\widehat{\boldsymbol{\omega}}_i$. In this equation, the pressure vanished because its projection along $\boldsymbol{Q}$ implies the product of $\boldsymbol{Q}$ by $\boldsymbol{\xi}$ that is null.
Owing to relation (51), we can simplify the iterative scheme as follows:

initialization:	$\boldsymbol{v}_0 = \boldsymbol{V}$, $\boldsymbol{d}_0 = 0$
iteration i :	(a) $\boldsymbol{\omega}_i = \beta(\boldsymbol{x})\boldsymbol{v}^i$, $\boldsymbol{s}_i = 2\varphi(\boldsymbol{x})\boldsymbol{d}_i$
	(b) $\widehat{\boldsymbol{\omega}}_i = FFT(\boldsymbol{\omega}_i)$, $\widehat{\boldsymbol{s}}_i = FFT(\boldsymbol{s}_i)$
	(c) $\widehat{\boldsymbol{E}}_i = \boldsymbol{Q}.(i\widehat{\boldsymbol{s}}_i.\boldsymbol{\xi} - \widehat{\boldsymbol{\omega}}_i)$
	(d) convergence criterion
	(e) $\widehat{\boldsymbol{v}}_{i+1} = \widehat{\boldsymbol{v}}_i + \lambda\widehat{\boldsymbol{E}}_i$
	(f) $\widehat{\boldsymbol{d}}_{i+1} = i\widehat{\boldsymbol{v}}_{i+1} \otimes_s \boldsymbol{\xi}$
	(g) $\boldsymbol{v}_{i+1} = FFT^{-1}(\widehat{\boldsymbol{v}}_{i+1})$, $\boldsymbol{d}_{i+1} = FFT^{-1}(\widehat{\boldsymbol{d}}_{i+1})$

In the third form, it is not necessary to compute and to store the components of the Green tensor. This has the advantage to reduce the computer memory because the total number of components is 45. Indeed, the Green tensors $\boldsymbol{\Gamma}^0$, $\boldsymbol{\Omega}^0$, $\boldsymbol{G}^0$ possess 21, 18, and 6 distinct components respectively. With the third form, only the computation of λ and vector $\boldsymbol{E}$ (3 components) is required.
Note that the case of anisotropic porous solid could be considered by replacing, in step "a", the scalar $\beta(\boldsymbol{x})$ by a two order-tensor. If the porous solid is anisotropic, the local permeability k is replaced by a two-order tensor $\boldsymbol{k}$, and, in the definition of $\beta(\boldsymbol{x})$ given by (7), μk^1 is replaced by $\mu\boldsymbol{k}^{-1}$ involving the inverse of the two order permeability tensor $\boldsymbol{k}$.

4.5 The choice of the reference material

The convergence of the iterative scheme drastically depends upon the choice of the reference material. The latter is given by two coefficients φ_0 and β_0. The coefficients of the reference material is just introduced in order to obtain the convergence of the iterative scheme. In fact, φ_0 and β_0 could be interpreted as two preconditioners which are adjusted in order to obtain the better rate of convergence.
Following the methodology of Michel et al. (41) and Milton (42), the values of φ_0 and β_0 could be determined by minimizing the spectral radius of the linear operator involved by the Neumann series. In the context of elasticity, it has been demonstrated that the optimal elastic coefficients of the reference material are defined by the average of the local elastic coefficients of the phases (for a two phase composite). Milton (42) obtain a similar result for the heat problem.
It is possible to extend the demonstration in the case of the Brinkman equation. It is not provided here. In fact, we obtain an equivalent expression for φ_0 and β_0:

$$\varphi_0 = \frac{\varphi_p + \varphi_s}{2}, \quad \beta_0 = \frac{\beta_p + \beta_s}{2} \tag{53}$$

where the indices "p" and "s" make reference to the corresponding quantity taken in Ω_p and Ω_s respectively.

4.6 The convergence criterion

The convergence is achieved when the local equilibrium is satisfied. The local equilibrium is verified when the vector $\boldsymbol{E}_i$, given by Eq. (52), is null. The following convergence criterion is used to check the accuracy of our numerical solution:

$$\frac{\sqrt{\sum_n \|\boldsymbol{E}_i(\boldsymbol{\xi}_n)\|^2}}{\|\boldsymbol{W}_i\|} \leq \eta \tag{54}$$

where $\| \bullet \|$ is the L^2-norm for a vector and η is the precision.
The convergence of the iterative scheme is illustrated by considering the case of a circular macropore in a squared unit cell. The void radius is denoted by R. For the non dimensional problem, we define by $\overline{R} = R/l_1$ the normalized radius where it is recalled that l_1 is the dimension of the unit cell. The calculations are performed with $\overline{R} = 0.25$, the diameter of the circular hole is then half the dimension of the unit cell. The calculations are performed with 256×256 wave vectors. The FFT solution for the permeability is computed with different values of η and is compared with a solution computed with a precision of $\eta = 10^{-15}$. The relative error is reported in figure 2 for two values of ε. The results show that a very good precision is obtained by considering $\eta = 10^{-6}$.

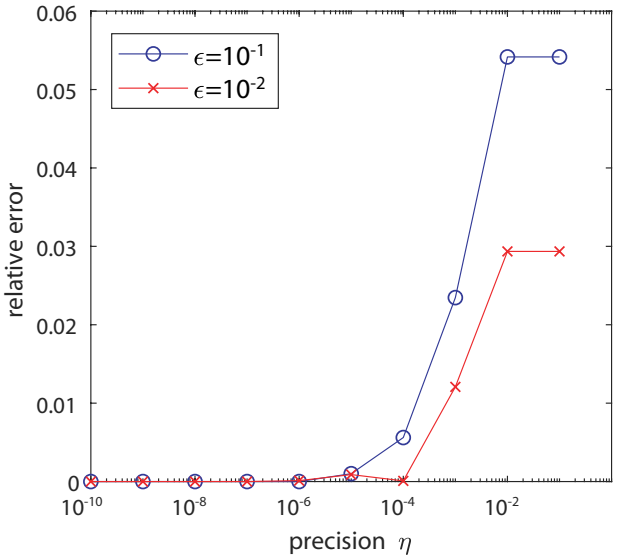

Fig. 2. Relative error for the permeability as function of the precision η. Case of a circular hole with $R = 0.25$.

5 Application to a biporous solid with circular macropores

5.1 Validation and comparisons with analytic solutions

Analytic solutions have been provided by Markov et al. (39). The principle of the approach consists in determining an equivalent permeability for a circular hole embedded in an infinite porous medium. Next, by making use of the analogy between the Darcy equation and that of the thermal conductivity, the effective permeability is estimated by the Maxwell formula.
The equivalent permeability obtained by Markov et al. (39) for a circular macropore is:

$$k' = \frac{R^2}{2}\left(1 - \frac{3\lambda\sqrt{k}}{R}\right) \tag{55}$$

in which λ is a coefficient of the Beaver-Joseph-Saffman (BJS) interface model. Markov et al. (39) suggests that the term with the coefficient λ in Eq. (55) is negligible and the permeability of the circular void could be approximated by $k' = R^2/2$. The justification is that $k = O(l_2^2)$ where l_2 is the characteristic dimension of the second porosity and then $\sqrt{k}/R = O(l_2/R)$ which must be a small parameter assuming the strict scale separation between the two populations of cavities. Moreover, Markov et al. (39) suggest that coefficient λ is comprised between 0 and 5. So, the term proportional to λ could be neglected. Note that the effective permeability of doubly porous materials with

cylindrical and spherical macropores has been recently provided by Monchiet et al. (49). The determination of the permeability of the equivalent Darcy solid has led to the following expression:

$$k' = \frac{R^2}{2}\left(1 + \frac{2\sqrt{k}}{\delta R}\right) \tag{56}$$

where $\delta = 1/\lambda$ is the slip coefficient. It must be observed that, by neglecting the term with δ, we obtain the same approximation: $k' = R^2/2$.
For the comparison with the FFT solutions based on the Brinkman equation, it is important to recall that the conditions at the interface are the continuity of the velocity and the traction and differ from the conditions given by the BJS model. Particularly, the case $\lambda = 0$ in the BJS model corresponds to the adherence, i.e. the tangential component of the velocity field is null at the frontier of the Stokes region but its counterpart in the Darcy region is not necessary null. Only the normal component of the velocity field is continuous across the interface. With the Brinkman model, both the normal and tangential components of the velocity are continuous.
The macroscopic permeability K is given by the Maxwell formula for a dilute suspension of conducting spheres in a conducting matrix (and by making the analogy between conductivity and permeability):

$$K = k\left(1 + 2f\frac{c-1}{1+f+c(1-f)}\right) \tag{57}$$

where c denotes the phase contrast defined by $c = k'/k$ that is, owing to eq. (55) with $\lambda = 0$:

$$c = \frac{R^2}{2k} \tag{58}$$

Using the hypothesis of strong separation of scales, the contrast is very large, $c >> 1$. The effective permeability can be approximated by taking the limit $c \to +\infty$ in Eq. (57) and leads to:

$$K = k\frac{1+f}{1-f} \tag{59}$$

We aim now to provide comparisons between the Maxwell formula for $c = +\infty$ and $c = R^2/(2k)$ with the FFT solution.
Note that the FFT method is implemented with the shape coefficient for the circular inclusion. The shape function is the exact analytic expression of the Fourier transform of the characteristic function of the phases which can be determined analytically for particular simple geometries. The method has the advantage to describe exactly the geometry of the microstructure and the details about its numerical integration can be found in the paper of Bonnet et al. (12) (see also Monchiet (47) which provides some additional details about the convolution product with the shape coefficients).

As an application purpose, we provide in Figs. 3 and 4 the normalized permeability K/k as function of the radius of the macropore for $\varepsilon = 10^{-2}$ and $\varepsilon = 10^{-1}$ respectively. The equivalent viscosity μ_e is null. In Fig. 3, we observe that the estimates with $c = +\infty$ or $c = R^2/(2k)$ leads to the same values for the macroscopic permeability. The estimates coincide with the FFT solution for $f < 0.5$ but a difference is noted for higher values of the volume fraction of the porosity. Regarding Fig. 4, we observe a good agreement between the FFT solution and the estimate with the infinite contrast. Moreover, the estimate with $c = R^2/(2k)$ is not accurate. To summarize, the estimate with the infinite contrast is the better approximation whatever the value of ε.

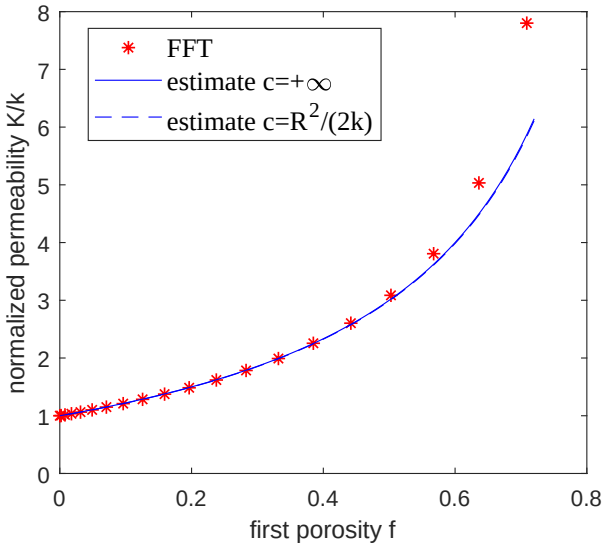

Fig. 3. Normalized macroscopic permeability K/k as function of the radius of the macropore. Comparison between the FFT solution and analytic estimates for $\varepsilon = 10^{-2}$.

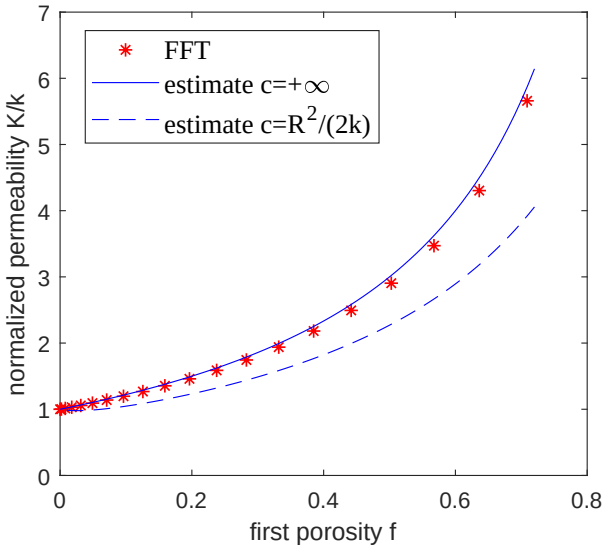

Fig. 4. Normalized macroscopic permeability K/k as function of the radius of the macropore. Comparison between the FFT solution and analytic estimates for $\varepsilon = 10^{-1}$.

The relative error between the analytic estimates of the macroscopic permeability and the FFT numerical solutions are provided on figure 5

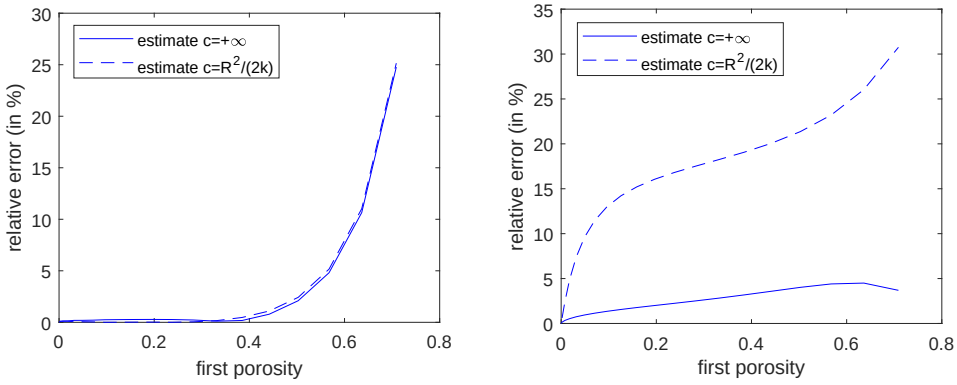

Fig. 5. Relative error (in percent) between the analytic solutions and the FFT numerical one in the $\varepsilon = 10^{-2}$ (at the left) and $\varepsilon = 10^{-1}$ (at the right).

As a validation, we compare our results with that provided by Golfier et al. (22) obtained with a commercial finite-element solver. The computations are performed with the pore radii $R = 0.1$, $R = 0.2$, $R = 0.3$, $R = 0.4$ and with an equivalent viscosity $\mu_e = \mu/\sqrt{3}$ (we consider the same value that in (22)). The variations of the non-dimensional macroscopic permeability K/k as function of the scale factor ε are shown in Fig. 6. We also represent the analytic estimate given by Eq. (59) that is independent of ε. We observe a very good agreement between the two numerical solutions in the case $R = 0.1$, $R = 0.2$,

$R = 0.3$. Moreover, the analytic solution is in a good agreement with the numerical solution at small values of ε. For the pore radius $R = 0.4$, we observe differences between the two numerical solutions and the analytic solution. The differences will probably be attributed to the boundary conditions.

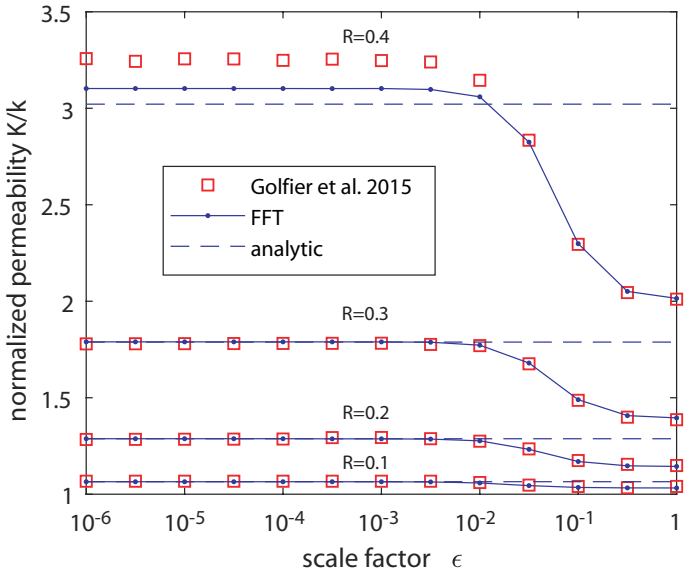

Fig. 6. Variations of the non-dimensional macroscopic permeability K/k as function of the scale factor ε. Comparison with the numerical solutions of Golfier et al. (22) and analytic estimate (59).

5.2 Simplification with an equivalent Darcy region

Knowing the equivalent permeability of the circular void, we can simulate the flow through the bi-porous solid by considering only the Darcy equation. Note that the Darcy equation is equivalent to the thermal conduction of composites and are closed to that of elasticity. As a consequence, standard FFT methods could be employed to solve the unit cell problem with two phases obeying to the Darcy equation. Note that the resolution of the problem with two Darcy regions could be also solved with the algorithm given in Table 4.4 by putting $\varphi(\boldsymbol{x}) = 0$ and by giving the corresponding expression for the resistivity $\beta(\boldsymbol{x})$ in each phase.

As an illustration purpose, the FFT solutions obtained with the Brinkman equation and with the Darcy equation are provided in Figs. 8 and 9. In these figures, we compare the effective permeability for $\varepsilon = 10^{-2}$ and $\varepsilon = 10^{-1}$. For the simulation with two Darcy regions, we use the equivalent permeability $k' = +\infty$ and $k' = R^2/2$ (that corresponding to the resistivities $h' = 0$ and $h' = 2/R^2$). In the case $\varepsilon = 10^{-2}$, we observe a very good agreement between the three results. For $\varepsilon = 10^{-1}$, the results corresponding to $c = +\infty$ is in a good agreement with that obtained with the Brinkman equation when

the volume fraction is inferior to 0.5 but overestimates the permeability for higher values of f. The results obtained with $c = R^2/(2k)$ underestimate the macroscopic permeability. These results are quite equivalent to those observed when making the comparison with the analytical estimates in the last section. Now we aim at comparing the local velocity field. We compare the results obtained with the Brinkman equation with that obtained with two Darcy solids and the equivalent permeability $k' = +\infty$. In Fig. 10, we provide the distribution of the velocity component v_1 along the line $x_1 = 0$ for the circular pore radii $R = 0.2$ and $R = 0.4$ and for $\varepsilon = 10^{-2}$, $\varepsilon = 10^{-1}$. In Fig. 11, we provide the same results for the velocity component v_1 but along the line $x_2 = 0$ (see Fig. 7). It is observed that the local solutions are very different especially within the macropore. In Fig. 10 a,b,d and in Fig. 11 a,b,d, the solutions out of the macropore are very closed but the solution within the macropore is different. Note that the porosity associated with the radii $R = 0.2$ and $R = 0.4$ is $f = 0.126$ and $f = 0.504$ respectively. For these porosity values, the macroscopic permeability computed with the Brinkman equation of the Darcy one are very closed (see Figs. 3 and 4) but the substitution with an equivalent Darcy region cannot be used to determine accurately the local solution.

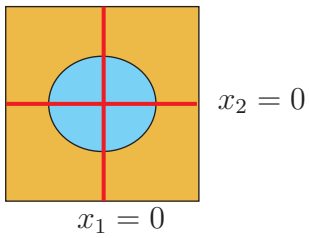

Fig. 7. Lines corresponding to $x_1 = 0$ and $x_2 = 0$.

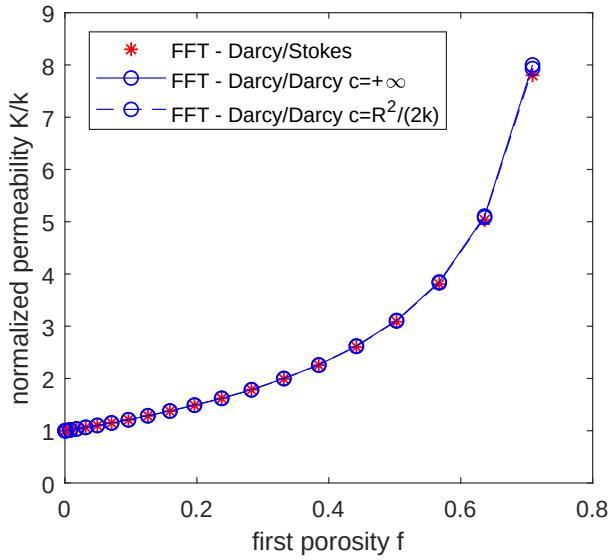

Fig. 8. Normalized macroscopic permeability K/k as function of the radius of the macropore. Comparison between the FFT solution and analytic estimates for $\varepsilon = 10^{-2}$.

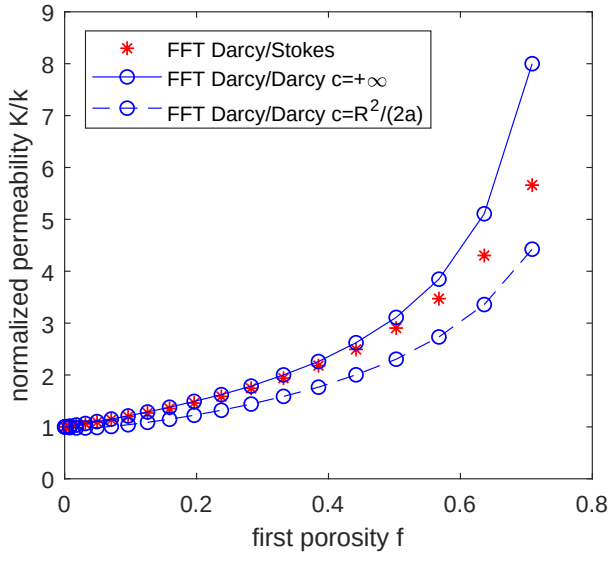

Fig. 9. Normalized macroscopic permeability K/k as function of the radius of the macropore. Comparison between the FFT solution and analytic estimates for $\varepsilon = 10^{-1}$.

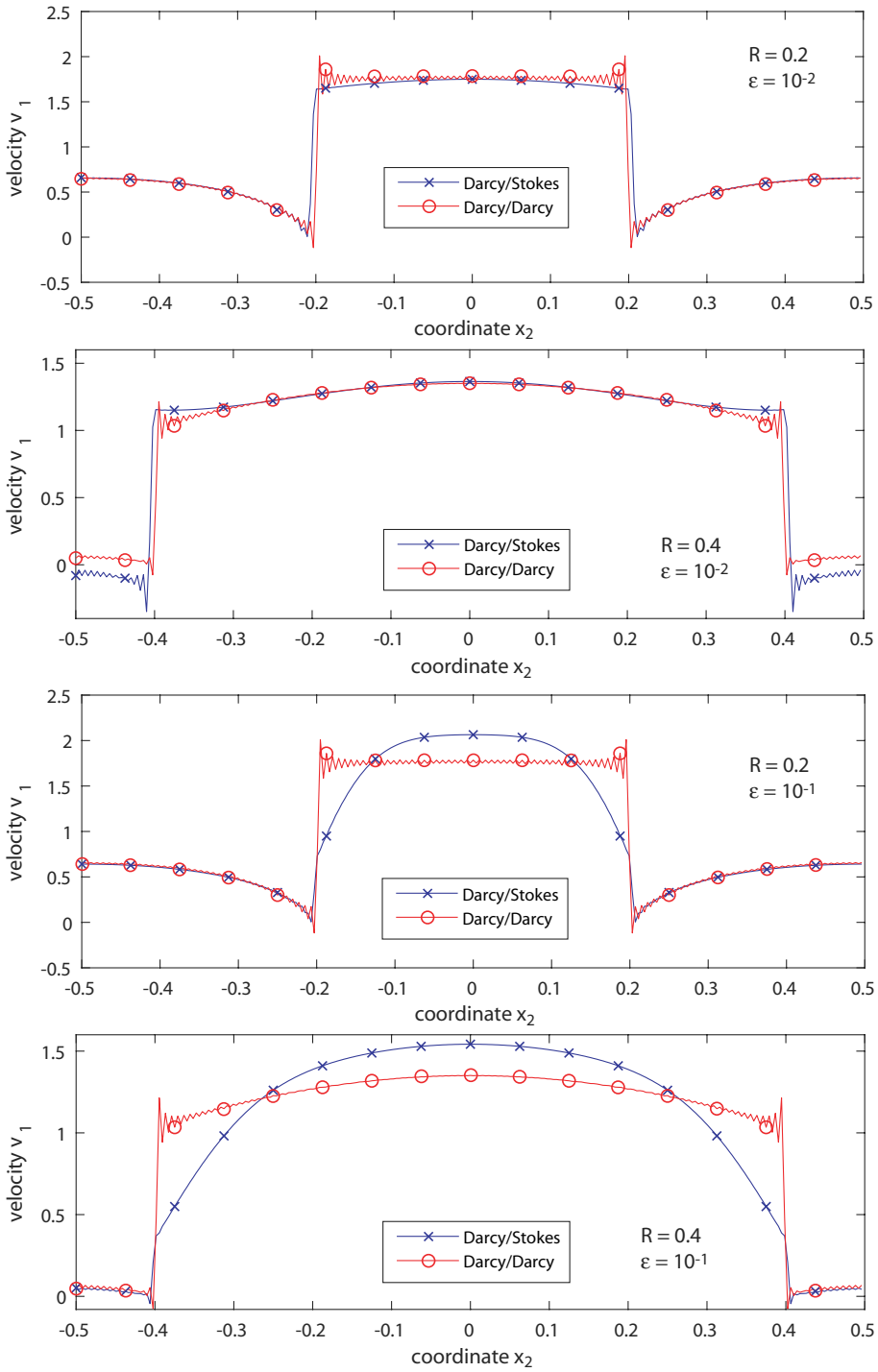

Fig. 10. Local velocity component v_1 along the line $x_1 = 0$.

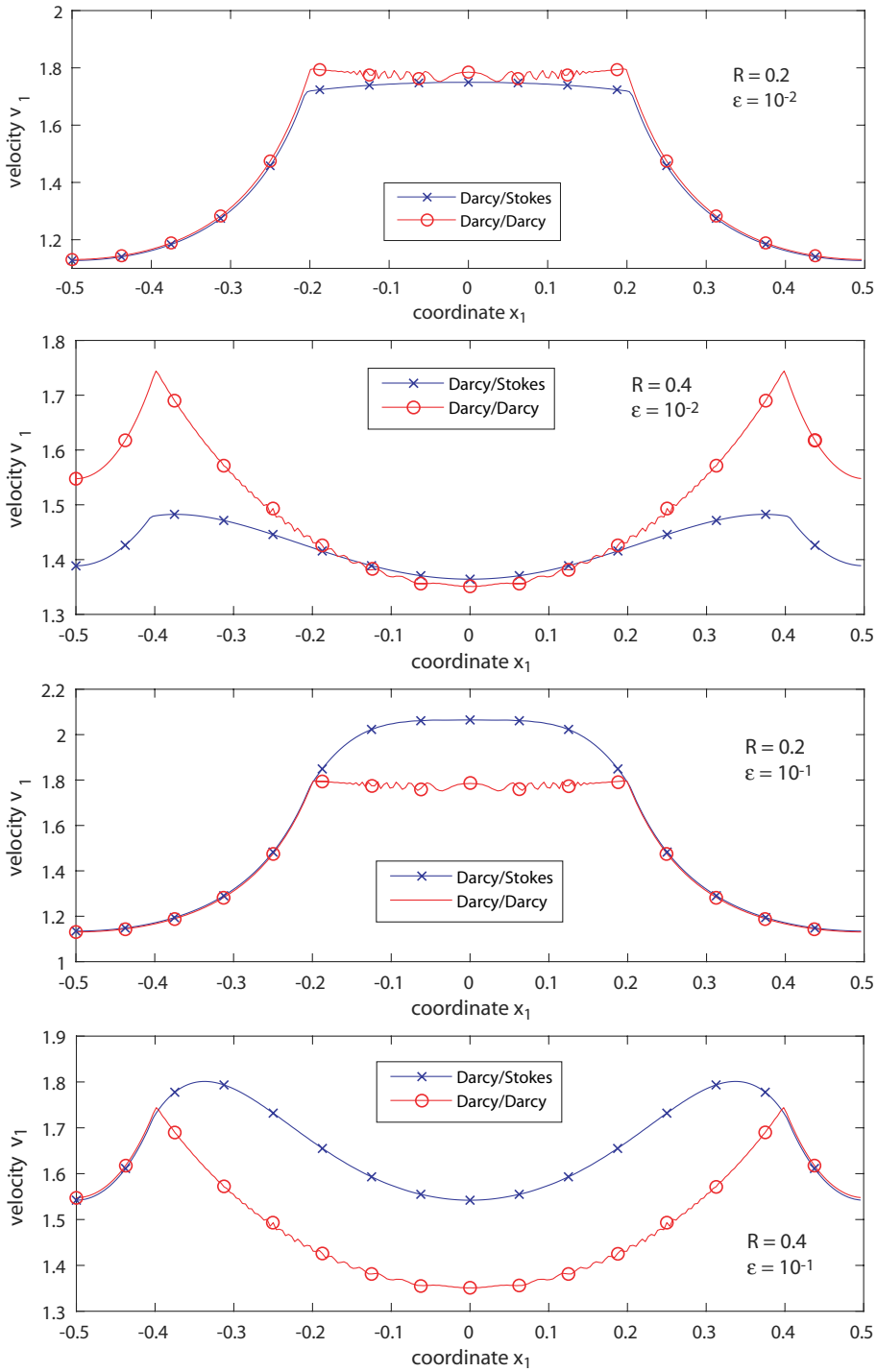

Fig. 11. Local velocity component v_1 along the line $x_2 = 0$.

6 Application to a biporous polymer

6.1 Elaboration of doubly porous polymeric materials

The doubly porous polymeric materials are elaborated via the double porogen templating approach. A 3-D continuous NaCl particle-based template leads to the first level of porosity, while the porogenic solvent ensures a lower porosity level through a phase separation process during the polymerization step. First, 2 g of NaCl particles having various sizes (from $50\mu m$ to $500\mu m$) are weighted in a glass vial and then gently stirred over an orbital shaking plate in order to ensure homogeneous particle packing. 2-Hydroxyethyl methacrylate (HEMA) is used as the functional monomer and ethylene glycol dimethacrylate (EGDMA) as a crosslinking agent. In a second step, HEMA and EGDMA are mixed in a 70/30 molar ratio in the presence of the polymerization initiator, i.e. DMPA, and 80 vol. % of a porogenic solvent, i.e. propan-2-ol (with respect to the total comonomers volume). The mixture is added to the NaCl particle template, and the polymerization is conducted in a UV oven for 4 h at $365nm$. Once the polymerization completed, NaCl particles are removed by extraction with deionized water for 3 days (water is changed once a day). Upon porogen extraction, the samples are washed abundantly with water, and dried at room temperature under vacuum.

6.2 Observation of doubly porous polymeric materials microstructure by means of μCT

X-ray microtomography (μCT) is used to characterize the 3-D microstructure of the doubly porous networks prepared via the double porogen templating approach. The aim is to investigate the homogeneity of porosity as well as the pore shape and interconnectivity. The experimental protocol consists in sticking a cylindrical biporous polymer sample, about 1 cm in diameter, on top of a thin cylindrical holder, which is mounted on the rotating stage of the microtomograph. The imaging configuration is based on a Hamamatsu L10801 micro-focus reflection X-ray source (max. 230 kV and 200 W, min. spot size $5\mu m$) combined with a Varian 2520 at panel detector (1920×1536 pixels, pixel size: 127 μm, CSI scintillator). Table 1 shows the experimental conditions.

Voxel size (m)	8.75
Tension (kV)	25
Intensity (A)	400
Number of radiographic projections	1440
Reconstructed Volume (voxels)	$1840 \times 1840 \times 1270$
Scanning time (h)	10

Table 1
Experimental conditions for the ţCT observation

The image of the microstructure shows a rather homogeneous pore distribution and a porous network with large pore imprints of sizes similar to those of NaCl particles. The exploration of the 3-D image of the sample confirmed that the large pores are mostly isolated within the polymer matrix. The second porosity level is not observed due to the insufficient resolution of the images.

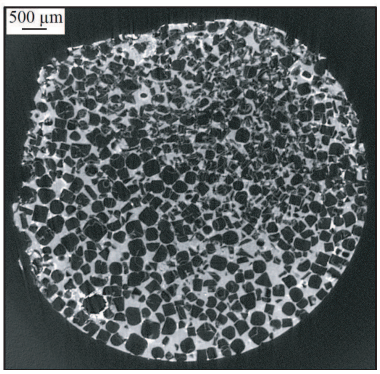

Fig. 12. X-ray microtomography of biporous polymer sample.

It must be also noted that some macropores are very closed and are separated by thin porous walls. It can be supposed that the walls are probably more porous that in the microporous matrix bulk. A zoom is provided in figure 13. The white circles show the walls between macropores in which the gray scale is higher than in the surrounded matrix.

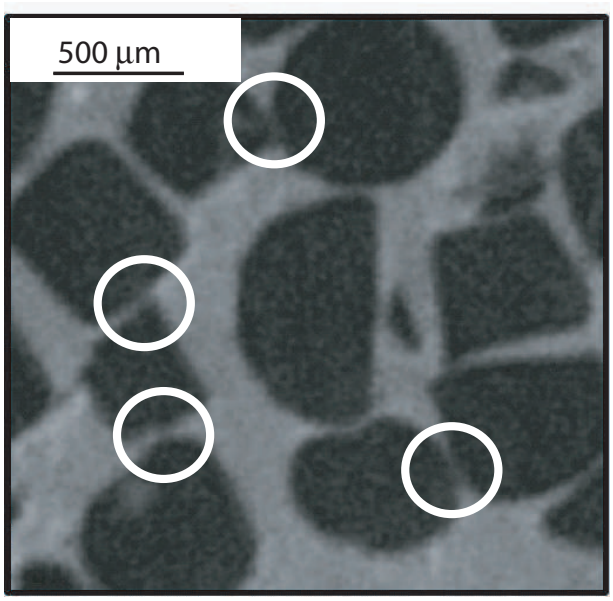

Fig. 13. Selected image of 186×186 pixels which shows the thin porous walls between the macropores

6.3 Thresholding of phases

In Fig. 14, at the right, we provide the distribution of pixels as a function of the grayscale. In these figures, two peaks are evident. Let us denote by X the value of the grayscale and by X_1, X_2 the values of X corresponding to the peaks. Each peak is associated with a phase, the fluid phase for the higher peak and the porous solid phase for the lower one. For FFT computations, we need to determine the thresholds below which the pixels are deemed to belong to the macropores and above which they are part of the porous solid phase. If we consider that some pixels are "mixed" or "composite", they are part of both the macropores and the porous solid phase, the introduction of two thresholds is then needed.
Let us then introduce two characteristic values X_1' and X_2'. When the grayscale X is inferior to X_1', then, the pixel belongs to the macropores. Alternatively, when $X > X_2'$, the pixel belongs to the porous phase. When X is comprised between X_1' and X_2', the pixel is mixed. The following law is then used to determine the volume fraction of the porous solid phase (c_s) and of the fluid phase (c_f) in a mixed pixel:

$$c_s(X) = \begin{cases} 0 & X < X'_1 \\ 1 & X > X'_2 \\ \dfrac{X - X'_1}{X'_2 - X'_1} & X'_1 \leq X \leq X'_2 \end{cases} \quad , \quad c_f(X) = 1 - c_s(X) \tag{60}$$

The two thresholds X'_1 and X'_2 are determined as function of the two values at the peak (X_1 and X_2) by the following relations:

$$X'_1 = (1-\alpha)X_1 + \alpha X_2 \tag{61}$$
$$X'_2 = \alpha X_1 + (1-\alpha)X_2 \tag{62}$$

in which α is a coefficient which must be taken in the range $[0, 0.5]$. The value of α determines the number of mixed pixels. When $\alpha = 0.5$, we have $X'_1 = X'_2 = (X_1 + X_2)/2$. There is only one threshold which separates the pixels which belong to the porous solid an fluid phases. In this case, there is no mixed pixels. When $\alpha = 0$, $X_1 = X'_1$ and $X_2 = X'_2$, the two thresholds are taken at the peaks and all the pixels lying between the peaks are mixed.

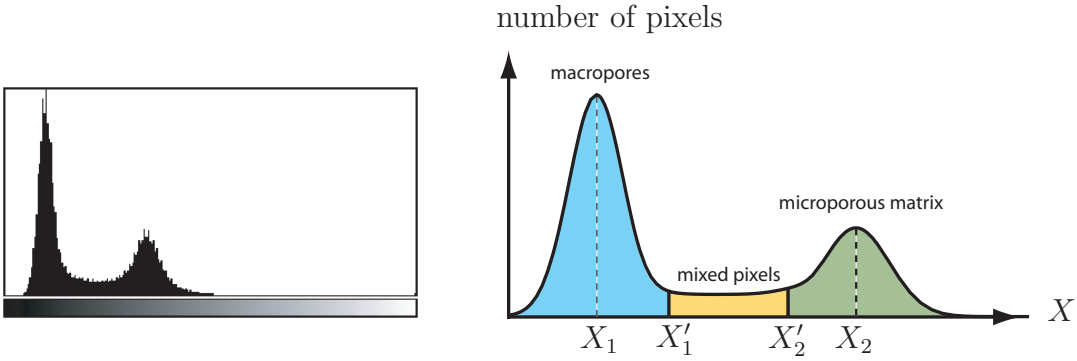

Fig. 14. At the left : number of pixels as function of the gray value. At the right : thresholding of the phases.

Some examples of slices from the data set at this level of thresholding are illustrated in Fig. 15 for three values of α. The images give the distribution of c_s for a selected image. The dark blue pixels belong to the macropores (fluid phase) in which c_s is null, the yellow pixels belong to the microporous solid in which c_s is equal to 1, the light blue pixels are mixed. It can be observed that all the mixed pixels are essentially located at the interface between the phases. The number of mixed pixels is maximal for $\alpha = 0$ and null when $\alpha = 0.5$. The value $\alpha = 0$ seems to be not pertinent since we observe some mixed pixels within the volume of the macropores while they should be confined next to the interface. For $\alpha = 0.5$, there is no pixels, this situation is not representative of the real microstructure because the walls between the macropores are more porous than in the bulk matrix. The intermediate value $\alpha = 0.25$ appears to lead to the more realistic distribution of c_f and is used for the calculations.

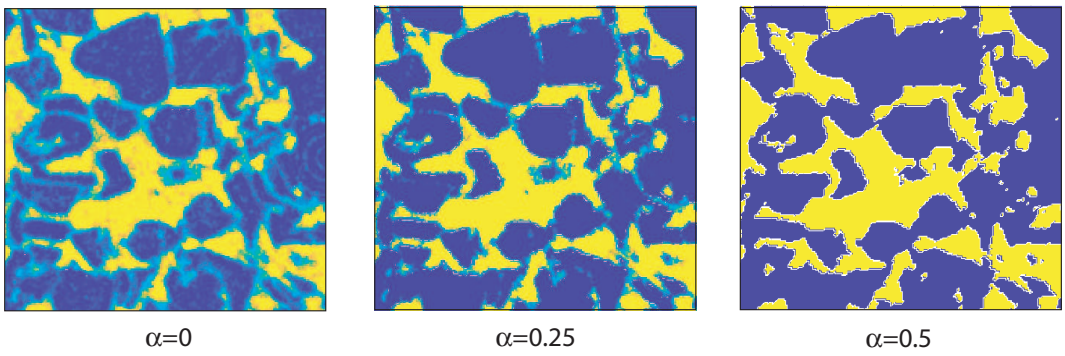

Fig. 15. Value of c_s for three values of the thresholding coefficient α for a selected slice of dimension 400×400.

6.4 Numerical results

We investigate the effect of the scale factor ε between the two population of pores. The calculations are performed on a unit cell of dimension 200^3 (see Fig. 16). The permeability is computed by increasing the value of ε from 10^{-3} to 10^{-1}, by doing so we gradually increase the smaller pores size while the size of the macropores is fixed. Note that for $\varepsilon > 10^{-1}$, the problem is not homogenizable because the sizes of the two populations are too close. For the values inferior to 10^{-3}, the time computations is prohibitive due to a lower rate of convergence of the iterative scheme. The method could by surely improved by considering accelerated schemes (see (44; 45; 46)) or the conjugate gradient (76) but this is not investigated in the present study.
Fig. 17 provides the dimensionless resistivity as function of ε. It is observed that the resistivity components increases with the scale factor. The macroscopic permeability then decreases with ε. This suggests that the larger the size of the macropores (in comparison to that of the micropores), the higher their influence on the macroscopic permeability. A physical meaning can be found by considering the dimensionless problem (see Eq. (14) together with (16)). The apparent viscosity in the macropores (that is ε^2) decreases when the scale factor also decreases and consequently, the velocity in the macropores increases when the size of the micropores is reduced.

Fig. 16. 3d unit cell of the biporous polymer

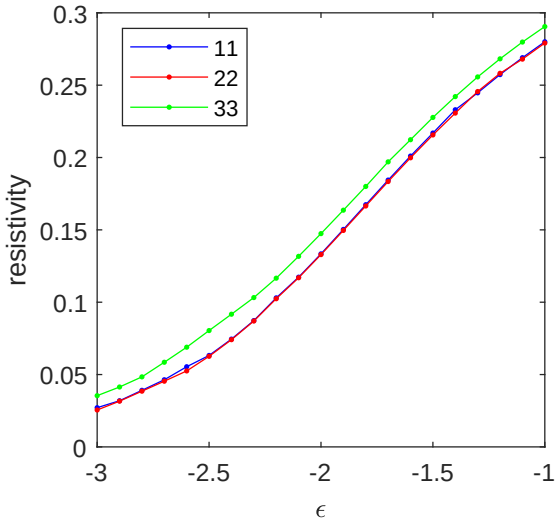

Fig. 17. Variation of the components of the macroscopic resistivity as function of the scale factor ε.

7 Conclusion

This paper proposes an efficient FFT-based iterative scheme to compute the local fluid flow and the overall transport properties of a porous solid with two populations of cavities. The fluid flow is described by the Darcy equation in the porous solid containing the micropores and by the Stokes equation in the macropores. The principle of the method is to use the Brinkmann equation

for both phases and the associated Green operator. The method of resolution uses an iterative scheme to solve the associated integral equation and the FFT to make the convolution product with the Green operator. The method has been first applied to the case of a porous solid containing a periodic distribution of circular macropores. The results are compared with analytic solutions and numerical FFT solutions with using an equivalent Darcy solid in place of the Stokes region. It has be found that the approximation with an equivalent Darcy solid (with an infinite permeability) can reproduce the variations of the effective permeability with the volume fraction of macropores. However, the results show that the method could not be applied to compute accurately the local velocity. Next, we apply the method to a biporous polymer. The computations are performed on digital images obtained by microtomography. The influence of the thresholding of the phases on the mass transport properties has been first studied. The proposed method consists in introducing two thresholds to define the pixels which belongs to the microporous region, the macropores or which are mixed. Depending on the thresholding coefficient variations some macropores can be connected of separated by a thin porous wall, leading to important variations on the macroscopic resistivity of the porous polymer. Next, the macroscopic resistivity is computed by increasing the size of the unit cell and making statistical averages for a finite number of selected images. Finally, calculations are performed on a 3D unit cell of the bi-porous polymer to analyze the effect of the scale factor between the populations of cavities. Through these applications, the proposed FFT method has proved to be an efficient approach to analyse the mass transfer properties through complex bi-porous microstructures. The approach could be applied to other problems such that fractured rocks or concrete. The approach could be also improved by introducing a refine description of mass transfer through the interface between the microporous matrix and the macropores adopting for instance the Beavers-Joseph-Saffman condition (7; 63) or by adding more terms in the momentum transport equation following (54; 55).

Acknowledgment

This work has benefited from a French government grant by ANR within the frame of the national program Investments for the Future ANR-11-LABX-022-01 (LabEx MMCD project).
The authors declare that they have no conflict of interest.

References

[1] **Arbogast T. and Brunson D.S.**
A computatonal method for approximating a Darcy-Stokes system gov-

erning a vuggy porous medium. *Comput. Geosciences*. 2007, vol. 11(3), pp. 207-218.

[2] **Auriault J.L. and Boutin C.**
Deformable porous media with double porosity. Quasi-statics. I: Coupling effects. *Transport in Porous Media*. 1992, vol. 7, pp. 63-82.

[3] **Auriault J.L. and Boutin C.**
Deformable porous media with double porosity. Quasi-statics. II: Memory effects. *Transport in Porous Media*. 1993, vol. 10, pp. 153-169.

[4] **Auriault J.L. and Boutin C.**
Deformable porous media with double porosity. III: Acoustics. *Transport in Porous Media*. 1994, vol. 14, pp. 143-162.

[5] **Auriault J.-L., Boutin C., and Geindreau C.**
Homogenization of coupled phenomena in heterogenous media, Wiley-ISTE, London, 2009.

[6] **Babuska I.**
Error-bounds for finite element method. *Numerische Mathematik* 1971, vol. 16, pp. 322-333.

[7] **Beavers G.S. and Joseph D.D.**
Boundary condition at a naturally permeable wall. *J. Fluid Mech.* 1967, vol. 30(1), pp. 197-207.

[8] **Beckermann C., Ramadhyani S. and Viskanta R.**
Natural convection flow and heat transfer between a fluid layer and a porous layer inside a rectangular enclosure. *Journal of Heat Transfer.* 1987, vol. 109, pp. 363-370.

[9] **Beckermann C., Viskanta R. and Ramadhyani S.**
Natural convection in vertical enclosures containing simultaneously fluid and porous layers. *Journal of Fluid Mechanics.* 1988, vol. 186, pp. 257-284.

[10] **Bensoussan A., Lions J., Papanicolaou G.**
Asymptotic analysis for periodic structures. North-Holland, Amsterdam. 1978.

[11] **Bernardi C., Hecht F. and Pironneau O.**
Coupling Darcy and Stokes equations for porous media with cracks. *ESAIM: Mathematical Modelling and Numerical Analysis.* 2005, vol. 39(1), pp. 7-35.

[12] **Bonnet G.**
Effective properties of elastic periodic composite media with fibers. *J. Mech. Phys. Solids.* 2007, vol. 55, pp. 881-899.

[13] **Boutin C., Royer P. and Auriault J.L.**
Acoustic absorption of porous surfacing with dual porosity. *Int. J. Solids Structures.* 1998, vol. 34, pp. 4709-4737.

[14] **Brezzi F.**
On the existence, uniqueness and approximation of saddle-point problems arising from lagrangian multipliers. *Revue française d'automatique, informatique, recherche opérationnelle. Analyse numérique.* 1974, vol. 8,

pp. 129-151.

[15] **Brinkman H.C.**
A calculation of the viscous force exerted by a flowing fluid on a dense swarm of particles. *App. Sci. Res.* 1949, vol. 1, pp. 27-34.

[16] **Brinkman H.C.**
On the permeability of media consisting of closely packed porous particles. *App. Sci. Res.* 1949, vol. 1, pp. 81-86.

[17] **Brown W.**
Solid mixture permittivities. *J. Comput. Math.* 1955, vol. 23, pp. 1514-1517.

[18] **Celle P., Drapier S. and Bergheau J.-M.**
Numerical modelling of liquid infusion into fibrous media undergoing compaction. *European Journal of Mechanics-A/Solids* 2008, vol. 27, pp. 647-661.

[19] **Correa M. and Loula A.**
A unified mixed formulation naturally coupling Stokes and Darcy flows. *Computer Methods in Applied Mechanics and Engineering.* 2009, vol. 198, pp. 2710-2722.

[20] **Discacciati M., Quarteroni A. and Valli A.**
Robin-robin domain decomposition methods for the Stokes-Darcy coupling. *SIAM Journal on Numerical Analysis* 2007, vol. 45, pp. 1246-1268.

[21] **Eshelby J.D.**
The determination of the elastic field of an ellipsoidal inclusion and related problem. *Proc. R. Soc. Lond.* 1957, A 241, 376-396.

[22] **Golfier F., Lasseux D., Quintard M.**
Investigation of the effective permeability of vuggy or fractured porous media from a Darcy-Brinkman approach. *Comput. Geosciences.* 2015, vol. 19, pp. 63-78.

[23] **Goyeau B., Lhuillier D., Gobin D., Velarde M.G.**
Momentum transport at a fluid-porous interface. *Int. J. Heat and Mass Transfer.* 2003, vol. 46, pp. 4071-4081.

[24] **Hanspal N. S., Waghode A. N., Nassehi V. and Wakemann R.J.**
Numerical analysis of coupled Stokes/Darcy flows in industrial filtrations *Transport in Porous Media.* 2006, vol. 64, pp. 73-101.

[25] **Hornung U.**
Homogenization and porous media. *Interdisciplinary Applied Mathematics Series.* Springer-Verlag, Berlin Heidelberg New York. 1997.

[26] **Jones I.**
Low Reynolds number flow past a porous spherical shell. *Mathematical Proceedings of the Cambridge Philosophical Society. Cambridge Univ Press.* 1973, vol. 73, pp. 231-238.

[27] **Joodi A.S., Sizaret S., Binet S., Bruand A., Alberic P., Lepiller M.** Development of a Darcy-Brinkman model to simulate water flow and tracer transport in a heterogeneous karstic aquifer (Val d'Orléans, France). *Hydrogeology journal.* 2010, vol. 18(2), pp. 295-309.

[28] **Jiang R., Zhang C., Cui Y., Wang Q., Zhang W., Zhang F.**
Characteristics of transient pressure performance of horizontal wells in fractured-vuggy tight fractal reservoirs considering nonlinear seepage. *Oil Gas Sci. Technol. - Rev. IFP Energies nouvelles.* 2019, vol. 74, nb. 57.

[29] **Joseph D. D. and Tao L.**
Lubrication of a porous bearing-Stokes solution. *Journal of Applied Mechanics.* 1966, vol. 33, pp. 753-760.

[30] **Kanit T., Forest S., Galliet I., Mounoury V. and Jeulin D.**
Determination of the size of the representative volume element for random composites: statistical and numerical approach. *International Journal of Solids and Structures* 2003, vol. 40, issue.13-14, pp. 3647-3679.

[31] **Karper T., Mardal K.-A. and Winther R.**
Unified finite element discretizations of coupled Darcy-Stokes flow. *Numerical Methods for Partial Differential Equations.* 2009, vol. 25, pp. 311-326.

[32] **Kroner E.**
Statistical Continuum Mechanics (Springer-Verlag, Wien, 1972).

[33] **Layton W.J., Schieweck F. and Yotov I.**
Coupling fluid flow with porous media flow. *SIAM J. Appl. Math.* 2000, vol. 60, pp. 2195-2218.

[34] **Li Y., Fu Z.-Y and Su B.-L.**
Hierarchically structured porous materials for energy conversion and storage. *Adv. Funct. Mater.*. 2012, vol. 22, pp. 4634-4667.

[35] **Liu X.H. and Ma P.X.**
Polymeric scaffolds for bone tissue engineering. *Annals of Biomedical Engineering.* 2004, vol. 32, pp. 477-486.

[36] **Luminari N., Zampogna G.A., Airiau C., Bottaro A.**
A penalization method to treat the interface between a free-fluid region and a fibrous medium. *J. Porous Media.* 2019, vol. 22(9), pp. 1095-1107.

[37] **Lundgren T.S.**
Slow flow through stationary random beds and suspensions of spheres. *Journal of Fluid Mechanics.* 1972, vol. 51, pp. 273-299.

[38] **Ly H.-B., Monchiet V. and Grande D.**
Computation of permeability with Fast Fourier Transform from 3d digital images of microstructures. *Int. J. Num. Meth. Heat and Fluid Flow.* 2016, vol. 26(5), pp. 1328-1345.

[39] **Markov M., Kazatchenko E., Mousatov A., Pervago E.**
Permeability of the fluid-filled inclusions in porous media. Transp. Porous Med. 2010, vol. 84, pp. 307-317.

[40] **Mauoka T.**
Convective currents in a horizontal layer divided by a permeable wall. *Bulletin of JSME.* 1974, vol. 17, pp. 225-232.

[41] **Michel J. C., Moulinec H. and Suquet P.**
A computational scheme for linear and non-linear composites with ar-

bitrary phase contrast. *Int. J. Numer. Meth. Engng.* 2001, vol. 52, pp. 139-160.

[42] **Milton G. W.**
The Theory of Composites. Cambridge University Press, 2002.

[43] **Monchiet V., Bonnet G. and Lauriat G.**
A FFT-based method to compute the permeability induced by a Stokes slip flow through a porous medium. *Comptes Rendus Mécanique.* 2009, vol. 337(4), pp. 192-197.

[44] **Monchiet V. and Bonnet G.**
A polarization based FFT iterative scheme for computing the effective properties of elastic composites with arbitrary contrast. *Int. J. Num. Meth. Engrg.* 2012, vol. 89(11), pp. 1419-1436.

[45] **Monchiet V. and Bonnet G.**
A polarization-based fast numerical method for computing the effective conductivity of composites. *Int. Journal of Num. Meth. Heat and Fluid Flow.* 2013, vol. 23(7), pp. 1256-1271.

[46] **Monchiet V., Bonnet G.**
Numerical homogenization of non linear composites with a polarization-based FFT iterative scheme. *Comput. Material Science.* 2013, vol. 79, pp. 276-283.

[47] **Monchiet V.**
Combining FFT methods and variational principles to compute bounds and estimates for the properties of elastic composites. *Comput. Meth. Appl. Mech. Engrg.* 2015, vol. 283, pp. 454-473.

[48] **Monchiet V.** FFT based iterative schemes for composites conductors with non-overlapping fibers and Kapitza interface resistance. *Int. J. Solids Struct.* 2018, vol. 135, pp. 14-25.

[49] **Monchiet V., Ly H.-B., Grande. D.**
Macroscopic permeability of doubly porous materials with cylindrical and spherical macropores. Meccanica. 2019, vol. 54(10), pp. 1583-1596.

[50] **Moulinec H. and Suquet P.**
A fast numerical method for computing the linear and nonlinear mechanical properties of composites. *C. R. Acad. Sci.* 1994, vol. 318(11), pp. 1417-1423.

[51] **Mura T.**.
Micromechanics of Defects in Solids. Martinus Nijhoff, Dordrecht. 1987.

[52] **Neale G., Epstein N. and Nader W.**
Creeping flow relative to permeable spheres. *Chem. Engrg. Science.* 1973, vol. 28, pp. 1865-1874.

[53] **Neale G. H. and Nader W. K.**
Prediction of transport processes within porous media: creeping flow relative to a fixed swarm of spherical particles. *AIChE Journal* 1974, vol. 20, pp. 530-538.

[54] **Ochoa-Tapia J.A., Whitaker S.**
Momentum transfer at the boundary between a porous medium and a ho-

mogeneous fluid. I. theorethical development. *Int. J. Heat Mass Transf.*. 1995, vol. 38(14), pp. 2635-2646.

[55] **Ochoa-Tapia J.A., Whitaker S.**
Momentum transfer at the boundary between a porous medium and a homogeneous fluid. II. comparison with experiment. *Int. J. Heat Mass Transf.*. 1995, vol. 38(14), pp. 2647-2655.

[56] **Olny X. and Boutin C.**
Acoustic wave propagation in double porosity media. *J. Acoust. Soc. Am.* 2003, vol. 114(1), pp. 73-89.

[57] **Popov P., Qin G., Bi L., Efendiev Y., Ewing R., Li J., Efendiev Y., Kang Z. and Li J.**
Multiphysics and multiscale methods for modeling fluid flow through naturally fractured carbonate karst reservoirs. *SPE Reservoir Evaluation & Engineering*. 2009, vol. 12(2), pp. 218-231.

[58] **Poulikakos D. and Kazmierczak M.**
Forced convection in a duct partially filled with a porous material. *ASME J. Heat Transfer* 1987, vol. 109, pp. 653-662.

[59] **Poupart R., Grande D., Carbonnier B., Le Droumaguet B.**
Porous polymers and metallic nanoparticles: A hybrid wedding as a robust method toward efficient supported catalytic systems. *Progress in Polymer Science*. 2019, vol. 96, pp. 21-42.

[60] **Quintard M., Whitaker S.**
Transport in chemically and mechanically heterogeneous porous media-III. Large-scale mechanical equilibrium and the regional form of Darcy's law. *Advances in Water Resources*. 1998, vol. 21 (7), pp. 617-629.

[61] **Rasoulzadeh M., Kuchuk F.J.**
Effective Permeability of a porous medium with spherical and spheroidal vug and fracture inclusions *Transp Porous Med.* 2017, vol. 116, pp. 613-644.

[62] **Royer P., Auriault J.L. and Boutin C.**
Macroscopic modeling of double-porosity reservoirs. *Journal of Petroleum Science and Engineering.* 1996, vol. 16, pp. 187-202.

[63] **Saffman P.G.**
On the boundary condition at the interface of a porous medium. *Stud. Appl. Math.* 1971, vol. 1, pp. 93-101.

[64] **Salinger A.G., Aris R. and Derby J.J.**
Modeling the spontaneous ignition of coal stockpiles. *AIChE journal.* 1994, vol. 40, pp. 991-1004.

[65] **Sanchez-Palencia, E.**
Comportements local et macroscopique d'un type de milieux physiques hétérogènes. *Int. J. Eng. Sci.* 1974, vol. 12, pp. 331-351.

[66] **Sanchez-Palencia, E.**
Non-homogeneous media and vibration theory. Berlin, Heidelberg, New York: Springer. 1980.

[67] **Silva G. and Ginzburg I.**

Stokes-Brinkman-Darcy solutions of bimodal porous flow across periodic array of permeable cylindrical inclusions: cell model, lubrication theory and LBM/FEM numerical simulations. *Transp. Porous Media.* 2016, vol. 111(3), pp. 795-825.

[68] **Su B.-L. , Sanchez C. and Yang X.Y.**
Hierarchically structured porous materials: From Nanoscience to Catalysis, Separation, Optics, Energy, and Life Science. *Wiley VCH.* 2011.

[69] **Sun M., Chen C., Chen L. and Su B.**
Hierarchically porous materials: Synthesis strategies and emerging applications. *Frontiers of Chemical Science and Engrg.* 2016, vol. 10(3), pp 301-347.

[70] **Tang H. and Fung Y.**
Fluid movement in a channel with permeable walls covered by porous media: a model of lung alveolar sheet. *J. Appl. Mech.* 1975, vol. 42, pp. 45-50.

[71] **Valdes-Parada F.J., Goyeau B., Ochoa-Tapia J.A.** Jump momentum boundary condition at a fluid-porous dividing surface: derivation of the closure problem. *Chem. Eng. Sci.* 2007, vol. 62, pp. 4025-4039.

[72] **Valdes-Parada F.J., Alvarez-Ramirez J., Goyeau B., Ochoa-Tapia J.A.** Computation of jump coefficients for momentum transfer between a porous medium and a fluid using a closed generalized transfer equation. *Transp Porous Med.* 2009, vol. 78, pp. 439-457.

[73] **Valdes-Parada F.J., Aguilar-Madera C.G., Ochoa-Tapia J.A., Goyeau B.** Velocity and stress jump conditions between a porous medium and a fluid. *Transp Porous Med.* 2013, vol. 78, pp. 439-457.

[74] **Wu D., Xu F., Sun B., Fu R., He H. and Matyjaszewski K.**
Design and preparation of porous polymers. *Chemical Reviews.* 2012, vol. 112, pp. 3959-4015.

[75] **Xie X., Xu J. and Xue G.**
Uniformly-stable finite element methods for Darcy-Stokes-Brinkman models. *J. Comput. Maths.*. 2008, vol. 26(3), pp. 437-455.

[76] **Zeman J., Vondrejc J., Novák J., Marek I.**
Accelerating a FFT-based solver for numerical homogenization of periodic media by conjugate gradients. *J. Comput. Physics.* 2010, vol. 229(21), pp. 8065-8071.

[77] **Zienkiewicz O. C., Taylor R. L., Zienkiewicz O. C. and Taylor R.L.**
The finite element method. McGraw-hill London. 1977, vol. 3.

A Derivation of the solution of the inclusion problem in Fourier space

Applying the Fourier transform to Eqs. (32), we obtain $\forall \boldsymbol{\xi} \neq 0$:

$$\begin{cases} i\widehat{\boldsymbol{\sigma}}.\boldsymbol{\xi} = \widehat{\boldsymbol{\omega}} \\ \widehat{\boldsymbol{\sigma}} = 2\varphi_0\widehat{\boldsymbol{d}} - \widehat{p}\boldsymbol{I} + \widehat{\boldsymbol{q}} \\ \widehat{\boldsymbol{\omega}} = \beta_0\widehat{\boldsymbol{v}} + \widehat{\boldsymbol{f}} \\ \widehat{\boldsymbol{d}} = i\widehat{\boldsymbol{v}} \otimes_s \boldsymbol{\xi} \\ i\widehat{\boldsymbol{v}}.\boldsymbol{\xi} = 0 \end{cases} \tag{A.1}$$

where the notation $\widehat{\boldsymbol{v}} \otimes_s \boldsymbol{\xi}$ represents the symmetrized tensorial product:

$$\widehat{\boldsymbol{v}} \otimes_s \boldsymbol{\xi} = \frac{1}{2}(\widehat{\boldsymbol{v}} \otimes \boldsymbol{\xi} + \boldsymbol{\xi} \otimes \widehat{\boldsymbol{v}}) \tag{A.2}$$

Owing to the incompressibility, $\widehat{\boldsymbol{v}}.\boldsymbol{\xi} = 0$, we deduce that the pressure reads:

$$\widehat{p} = -\frac{i}{\|\boldsymbol{\xi}\|}\boldsymbol{n}.\left[i\widehat{\boldsymbol{q}}.\boldsymbol{\xi} - \widehat{\boldsymbol{f}}\right] \tag{A.3}$$

and for the velocity:

$$\widehat{\boldsymbol{v}} = \frac{1}{\varphi_0\|\boldsymbol{\xi}\|^2 + \beta_0}\boldsymbol{Q}.\left[i\widehat{\boldsymbol{q}}.\boldsymbol{\xi} - \widehat{\boldsymbol{f}}\right] \tag{A.4}$$

in which $\boldsymbol{n}$ and $\boldsymbol{Q}$ are defined in Eq. .
The solution for the strain rate tensor is:

$$\begin{aligned} \widehat{\boldsymbol{d}} &= i\widehat{\boldsymbol{v}} \otimes_s \boldsymbol{\xi} \\ &= -\frac{1}{2(\varphi_0\|\boldsymbol{\xi}\|^2 + \beta_0)}\left\{\|\boldsymbol{\xi}\|^2(\boldsymbol{Q}.\widehat{\boldsymbol{q}}.\boldsymbol{P} + \boldsymbol{P}.\widehat{\boldsymbol{q}}.\boldsymbol{Q}) + 2i(\boldsymbol{Q}.\widehat{\boldsymbol{f}}) \otimes_s \boldsymbol{\xi}\right\} \end{aligned} \tag{A.5}$$

B Property of Green operator

We aim to simplify the product:

$$\widehat{\mathcal{G}}_0 \begin{pmatrix} 2\mu_0 \widehat{\boldsymbol{d}} \\ \gamma_0 \widehat{\boldsymbol{v}} \end{pmatrix} \tag{B.1}$$

for any pair of compatible field $\boldsymbol{d}$ and $\boldsymbol{v}$, i.e. related in the Fourier space by:

$$\widehat{\boldsymbol{d}} = i\widehat{\boldsymbol{v}} \otimes_s \boldsymbol{\xi} \tag{B.2}$$

To this purpose, we replace the green operator $\mathcal{G}_0$ by the expression given in Eq. (42). It follows that:

$$\widehat{\mathcal{G}}_0 \begin{pmatrix} 2\mu_0 \widehat{\boldsymbol{d}} \\ \gamma_0 \widehat{\boldsymbol{v}} \end{pmatrix} = \widehat{\mathcal{G}}_0 \begin{pmatrix} 2\mu_0 \widehat{\boldsymbol{\Gamma}}^0 : (i\widehat{\boldsymbol{v}} \otimes_s \boldsymbol{\xi}) + \gamma_0 \widehat{\boldsymbol{\Omega}}^0 . \widehat{\boldsymbol{v}} \\ -\overline{\boldsymbol{\Omega}^0} : (i\widehat{\boldsymbol{v}} \otimes_s \boldsymbol{\xi}) + \gamma_0 \boldsymbol{G}^0 . \widehat{\boldsymbol{v}} \end{pmatrix} \tag{B.3}$$

Considering the definitions provided in Eqs. (34)-(36) and after various simplifications, we obtain:

$$\widehat{\mathcal{G}}_0 \begin{pmatrix} 2\mu_0 \widehat{\boldsymbol{d}} \\ \gamma_0 \widehat{\boldsymbol{v}} \end{pmatrix} = \begin{pmatrix} i(\boldsymbol{Q}.\widehat{\boldsymbol{v}}) \otimes_s \boldsymbol{\xi} \\ \boldsymbol{Q}.\widehat{\boldsymbol{v}} \end{pmatrix} \tag{B.4}$$

Considering additionally the incompressibility, $\widehat{\boldsymbol{v}}.\boldsymbol{\xi} = 0$, we deduce that $\boldsymbol{Q}.\widehat{\boldsymbol{v}} = \widehat{\boldsymbol{v}}$ and $i(\boldsymbol{Q}.\widehat{\boldsymbol{v}}) \otimes_s \boldsymbol{\xi} = i\widehat{\boldsymbol{v}} \otimes_s \boldsymbol{\xi} = \widehat{\boldsymbol{d}}$. Coming back to the real space, we finally obtain:

$$\mathcal{G}_0 * \begin{pmatrix} 2\mu_0 \boldsymbol{d} \\ \gamma_0 \boldsymbol{v} \end{pmatrix} = \begin{pmatrix} \boldsymbol{d} \\ \boldsymbol{v} - \boldsymbol{V} \end{pmatrix} \tag{B.5}$$

where the volume average of each quantity has been eliminated because the Green operator is null for $\boldsymbol{\xi} = 0$. Therefore, the macroscopic velocity $\boldsymbol{V}$ has been subtracted to $\boldsymbol{v}$. The strain rate tensor $\boldsymbol{d}$ has a null volume average since it derivates from a periodic velocity field.